

Beyond maps: Patterns of formation processes at the Middle Pleistocene open-air site of Marathousa 1, Megalopolis Basin, Greece

D. Giusti^{a,*}, V. Tourloukis^a, G. E. Konidaris^a, N. Thompson^a, P. Karkanas^b, E. Panagopoulou^c, K. Harvati^a

^a*Paläoanthropologie, Senckenberg Centre for Human Evolution and Palaeoenvironment, Eberhard Karls Universität Tübingen, Rümelinstr. 23, 72070 Tübingen, Germany*

^b*Malcolm H. Wiener Laboratory for Archaeological Science, American School of Classical Studies at Athens, Greece*

^c*Ephoreia of Palaeoanthropology-Speleology of Greece, Athens, Greece*

Abstract

Recent excavations at the Middle Pleistocene open-air site of Marathousa 1 have unearthed in one of the two investigated areas (Area A) a partial skeleton of a single individual of *Palaeoloxodon antiquus* and other faunal remains in spatial and stratigraphic association with lithic artefacts. In Area B, a much higher number of lithic artefacts was collected, spatially and stratigraphically associated also with faunal remains. The two areas are stratigraphically correlated, the main fossiliferous layers representing an *en masse* depositional process in a lake margin context. Evidence of butchering (cut-marks) has been identified on bones of the elephant skeleton, as well on elephant and other mammal bones from Area B. However, due to the secondary deposition of the main find-bearing units, it is of primary importance to evaluate the degree and reliability of the spatial association of the lithic artefacts with the faunal remains. Indeed, spatial association does not necessarily imply causation, since natural syn- and post-depositional processes may equally produce spatial association. Assessing the degree and extent of post-depositional reworking processes is crucial to fully comprehend the archaeological record, and therefore to reliably interpret past human behaviours. The present study uses a comprehensive set of spatial statistics in order to disentangle the depositional processes behind the distribution of the archaeological and palaeontological record at Marathousa 1. Preliminary results of our analyses suggest minor reworking and substantial spatial association of the lithic and faunal assemblages, supporting the current interpretation of Marathousa 1 as a butchering site.

Keywords: Spatial analysis, Site formation processes, Vertical distribution, Fabric analysis, Point pattern analysis, Middle Pleistocene

*Corresponding author

Email address: domenico.giusti@uni-tuebingen.de (D. Giusti)

1 **1. Introduction**

2 Archaeological site formation processes, intensively studied since the early 1970s
3 (Isaac, 1967; Schiffer, 1972, 1983, 1987; Shackley, 1978; Wood and Johnson, 1978;
4 Binford, 1981; Schick, 1984, 1986, 1987; Petraglia and Nash, 1987; Petraglia and
5 Potts, 1994, among others), “still insufficiently taken in consideration” (Texier, 2000,
6 p.379) at the beginning of the 21st century, are nowadays fully acknowledged in the ar-
7 chaeological practice (Villa, 2004; Bailey, 2007; Brantingham et al., 2007; Malinsky-
8 Buller et al., 2011; Vaquero et al., 2012; Bargalló et al., 2016, among others). Drawing
9 inferences about past human behaviours from scatters of archaeological remains must
10 account for syn- and post-depositional contextual processes.

11 Several methods are currently applied in order to qualify and quantify the type and
12 degree of reworking of archaeological assemblages. Within the framework of a geoar-
13 chaeological and taphonomic approach, spatial statistics offer meaningful contributions
14 in unravelling site formation and modification processes from spatial patterns. How-
15 ever, while the spatio-temporal dimension is an ineluctable inherent property of any
16 biotic and abiotic process, spatial statistics are still insufficiently applied.

17 Distribution maps are cornerstones of the archaeological documentation process
18 and are primary analytic tools. However, their visual interpretation is prone to subjec-
19 tivity and is not reproducible (Bevan et al., 2013). Since the early 1970’s (see Hodder
20 and Orton (1976); Orton (1982) and references therein), the traditional, intuitive, ‘eye-
21 balling’ method of spotting spatial patterns has been abandoned in favour of more ob-
22 jective approaches, extensively borrowed from other fields. Nevertheless, quantitative
23 methods, while still percolating in the archaeological sciences from neighbouring dis-
24 ciplines, are not extensively used. Moreover, only a relatively small number of studies
25 have explicitly applied spatial point pattern analysis or geostatistics to the study of site
26 formation and modification processes (Lenoble et al., 2008; Domínguez-Rodrigo et al.,
27 2014b,a, 2017; Carrer, 2015; Giusti and Arzarello, 2016; Organista et al., 2017, but see
28 Hivernel and Hodder (1984) for an earlier work on the subject).

29 The goal of a taphonomic approach to spatial analysis is to move beyond distri-
30 bution maps by applying a comprehensive set of multiscale and multivariate spatial
31 statistics in order to reliably construct inferences from spatial patterns. An exhaustive
32 spatial analytic approach to archaeological inference, combined with a taphonomic
33 perspective, is essential for evaluating the depositional processes and integrity of the
34 archaeological assemblage, and consequently for a reliable interpretation of past hu-
35 man behaviours.

36 The present study uses a comprehensive set of spatial statistics in order to disentan-
37 gle the depositional processes behind the spatial distribution of the archaeological and
38 palaeontological record recovered during excavation at the Middle Pleistocene open-air
39 site of Marathousa 1, Megalopolis, Greece (Panagopoulou et al., 2015; Harvati et al.,
40 2016).

41 **1.1. Marathousa 1**

42 The site (Fig. 1), discovered in 2013 at the edge of an active lignite quarry, is
43 located between two lignite seams in the Pleistocene deposits of the Megalopolis basin,
44 Marathousa Member of the Choremi Formation (van Vugt et al., 2000). The regular

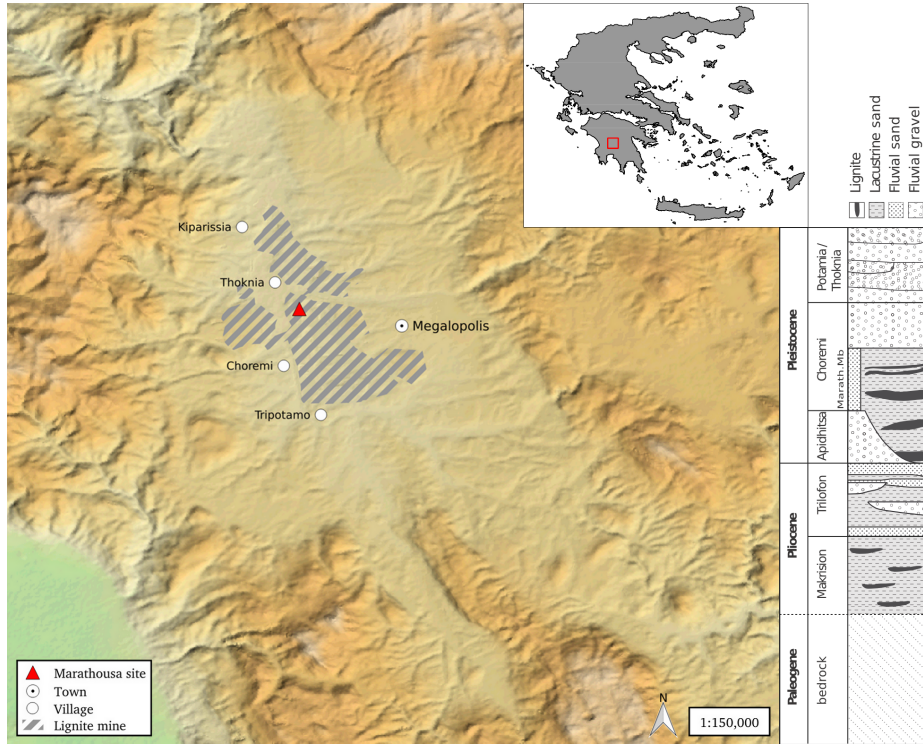


Figure 1: Geographical location of the Marathousa 1 site in the Megalopolis basin and stratigraphic column of the basin, modified after [van Vugt et al. \(2000\)](#).

45 alternation of lacustrine clay, silt and sand beds with lignite seams has been interpreted
 46 having cyclic glacial (or stadial) and interglacial (or interstadial) origin ([Nickel et al., 1996](#)). The half-graben configuration of the basin, with major subsidence along the
 47 NW-SE trending normal faults along the eastern margin, resulted in the gentle dip of
 48 the lake bottom at the opposite, western, margin of the lake, enabling the formation of
 49 swamps and the accumulation of organic material for prolonged periods of time ([van
 50 Vugt et al., 2000](#)).

51 Two excavation areas have been investigated since 2013 (Fig. 2): Area A, where
 52 several skeletal elements of a single individual of *Palaeoloxodon antiquus* have been
 53 unearthed, together with a number of lithic artefacts; and Area B, located 60 m to
 54 the South along the exposed section, where the lithic assemblage is richer and occurs
 55 in association with a faunal assemblage composed of isolated elephant bones, cervids
 56 and carnivores among others ([Konidaris et al., this issue](#); [Tourloukis et al., this issue](#)).
 57 Evidence of butchering (cut-marks) have been identified on two of the elephant bones
 58 from Area A, as well on elephant and other mammal bones from Area B ([Konidaris
 59 et al., this issue](#)).

60 The sedimentary sequence of the site (Fig. 3) includes lacustrine and fluvio-lacustrine
 61 clastic deposits sandwiched between two lignite seams (UA7-UB10 and UA1-UB1)

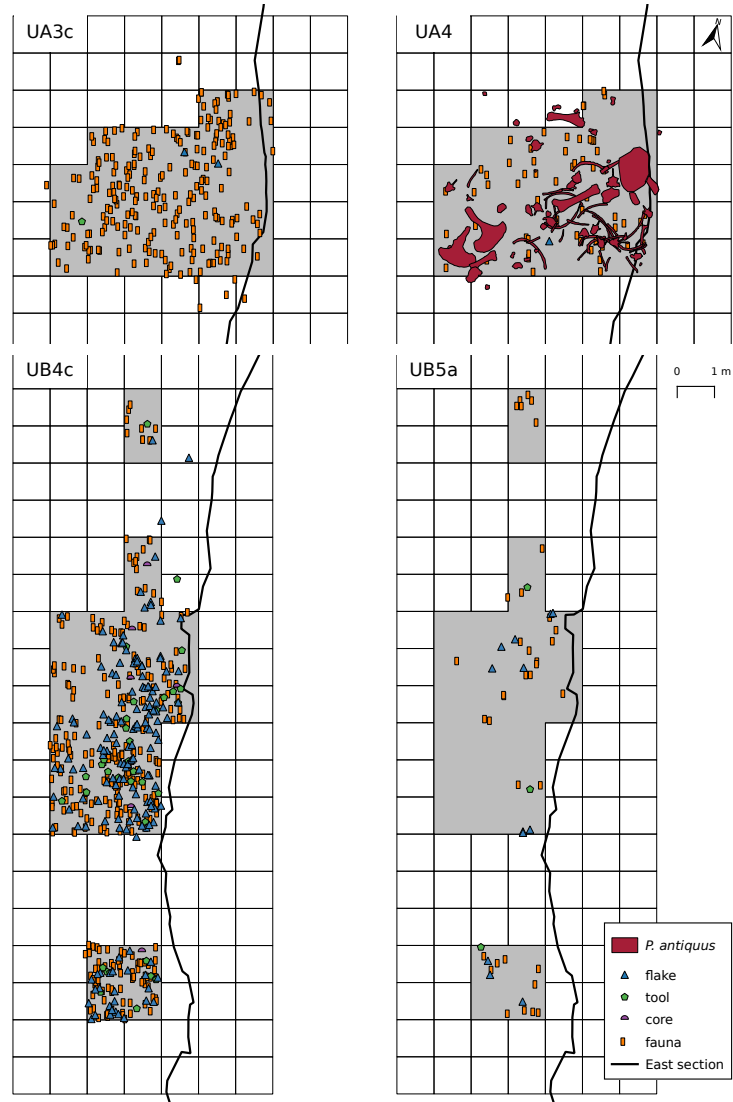


Figure 2: Distribution maps of the plotted remains from areas A (units UA3c and UA4) and B (units UB4c and UB5a). Grey zones mark the 2013-2015 excavation areas. The plotted remains of the *P. antiquus* skeleton were collected until 2016. Area B is located 60 m to the South, along the exposed East section of the lignite quarry.

(Karkanas et al., this issue). A major hiatus (contacts between UA3 and UA4, and between UB5 and UB6), attributed to exposure and erosion of a lake shore mudflat, divides the sequence in two parts. The lower part is characterised by relatively high rate sub-aqueous sedimentation of bedded sands and silts, containing low organic and carbonate content. The upper one is characterised by a series of erosional bounded depositional units, attributed to sub-aerial originated organic- and carbonate-rich mud flows and hyperconcentrated flows deposited at the margin of a swamp (Karkanas et al., this issue).

The erosional contacts UA3c/4 and UB4c/5a separate the two main find-bearing units in both areas (Fig. 3). In Area A, the elephant remains lie at the contact of UA3c/4 and are covered by UA3c (Fig. 4a); while in Area B, most of the remains were collected from unit UB4c (Figs. 2 and 4b). Units UA3c and UB4c (organic- and intraclast-rich silty sands) resemble dilute mud flows, showing a chaotic structure of rip-up clasts from the underlying unit, small-to-large wood fragments and rare rock clasts. In Area B, a relatively low number of remains was also found in massive organic-rich silty sands (UB5a, Fig. 2), which locally overlay channelised sands (UB5b/c), probably not preserved in Area A (Karkanas et al., this issue).

The flow event described above (units UA3c and UB4c), and specifically the erosional contacts between the fossiliferous horizons in the two areas (UA3c/4 and UB4c/5a), provide the essential background for the analysis and interpretation of the spatial distributions at Marathousa 1.

The secondary depositional nature of the main find horizons raises the question of how reliable is the spatial association between the lithic artefacts and the partial skeleton of a single *Palaeoloxodon antiquus* individual and other faunal remains. Since spatial association does not necessarily imply causation, and consequently synchrony, the answer has important consequences for the interpretation of the site in the broader context of the Middle Pleistocene human-proboscidean interactions. We aim to tackle this question and disentangle the formation processes acting at Marathousa 1 on the basis of spatial patterns through a three-prong spatial analytic approach:

1. by analysing, in a frame of references, the orientation patterns of remains from relevant stratigraphic units;
2. by quantifying and comparing their relative vertical distributions;
3. by identifying spatial trends in either the assemblage intensities and the associations between classes of remains.

Two contrasting models of deposition are tested: the autochthonous hypothesis (*sensu* Fernández-López, 1991; Domínguez-Rodrigo et al., 2012) states that the flow event, represented by units UA3c and UB4c, eroded and scoured the exposed surface (where the elephant was lying), thereby entraining clastic material (including artefacts) and re-depositing (*sensu* Fernández-López, 1991) this material at a close distance. This model implies the loss of any original, pristine spatial relations between remains, but minor transport from the primary depositional *loci*. On the other hand, the allochthonous hypothesis (*sensu* Fernández-López, 1991; Domínguez-Rodrigo et al., 2012) implies significant transport from the original *loci* of deposition and re-elaboration (*sensu* Fernández-López, 1991). According to this model, the spurious spatial associ-

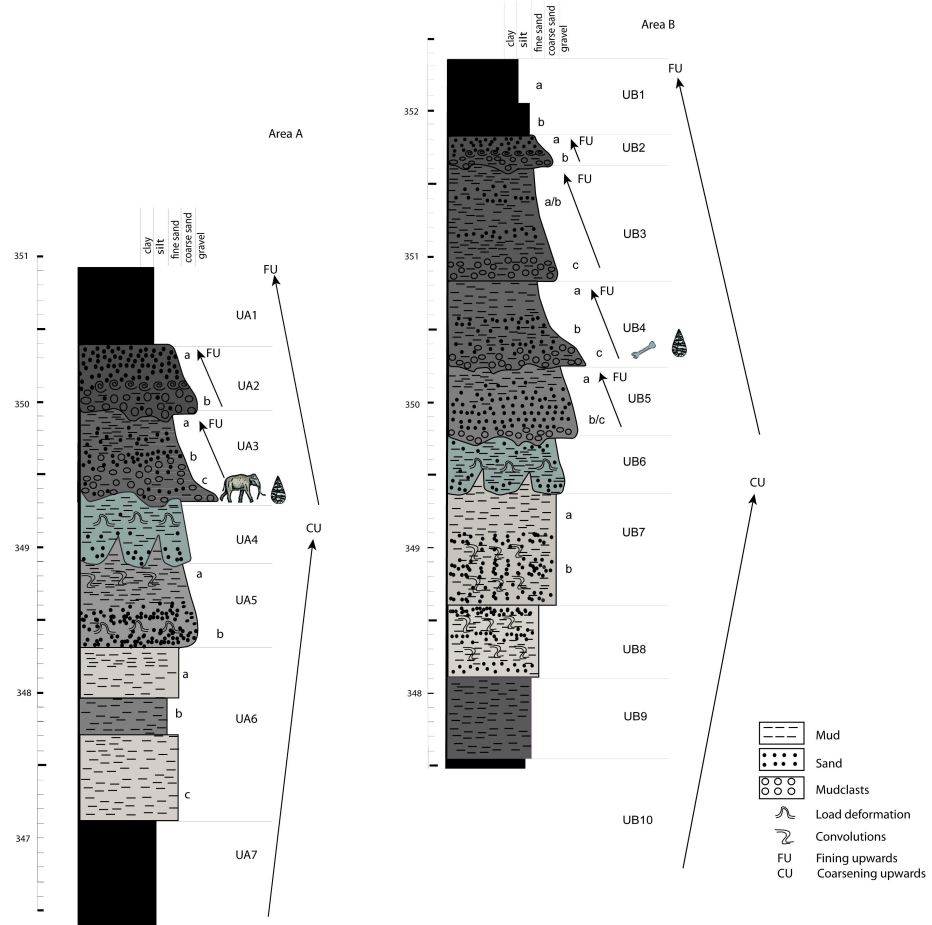


Figure 3: Stratigraphic setting of the Marathousa 1 site, modified after Karkanas et al. ([this issue](#)). Absolute elevations in m a.s.l.

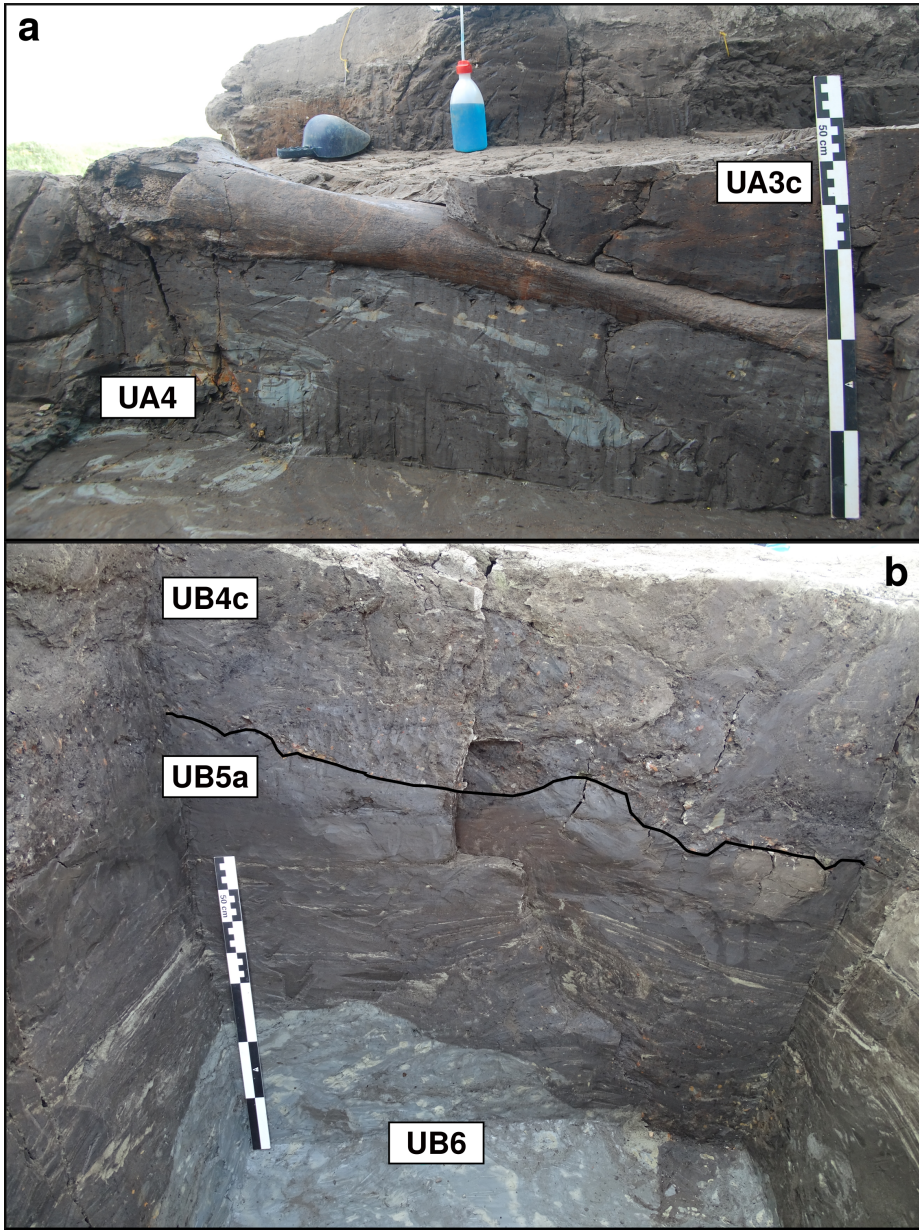


Figure 4: Photograph (2017) of the left femur of the *P. antiquus* skeleton, lying at the UA3c/4 contact and covered by unit UA3c (a). West profile (2014) of the excavation Area B (square 932/603), exposing the UB4c/5a (black solid line) and the UB5/6 erosional contacts (b).

107 ation between the lithic artefacts and faunal remains does not support any behavioural
108 interpretation.

109 **2. Material and methods**

110 Since 2013, systematic investigation of the Marathousa 1 site has been carried out
111 by a joint team from the Ephoreia of Palaeoanthropology-Speleology (Greek Ministry
112 of Culture) and the University of Tübingen. A grid system of 1 square meter units
113 was set up, oriented -14 degrees off the magnetic North, and including the two areas
114 of investigation. The excavation of the deposit proceeded in 50x50 cm sub-squares in
115 Area B and 1x1 m squares in Area A, and spits of 5 to 10 cm thickness, respectively.
116 Systematic water-screening of sediments was carried out on-site using 1 mm sieves
117 in order to guarantee recovery of the small-size fraction (e.g., micro-artefacts, small
118 mammal remains, fish, molluscs and small fragments of organic and inorganic mate-
119 rial). The three-dimensional coordinates of finds (i.e., all the lithic artefacts, teeth and
120 diagnostic bones; bones and organic material with a-axis ≥ 20 mm), collected spits
121 of sediment, samples and geological features (e.g., erosional contacts and mud cracks)
122 were recorded with a total station. Dense clouds of surface points of the elephant skele-
123 tal elements were acquired using both a total station and a close-range photogrammetric
124 technique.

125 The dimensions (length, width and thickness) of registered finds were measured
126 on-site with millimetre rules. Orientation (plunge and bearing) of elongated particles
127 (i.e., faunal remains, large wood fragments and lithic artefacts) was recorded since
128 2013 using a clock-like system (the bearing was measured, relatively to the grid North,
129 in twelve clockwise intervals of 30°; the plunge with a 22.5° accuracy). In 2015, the
130 use of a compass and inclinometer with an accuracy of 1° was introduced in Area B to
131 gradually replace the former method.

132 The widespread use of a compass and inclinometer to record orientation data (Voorhies,
133 Fiorillo, 1991; Bertran and Texier, 1995; Bertran et al., 1997; Lenoble and
134 Bertran, 2004; Eberth et al., 2007; Eren et al., 2010; Benito-Calvo et al., 2011; Domínguez-
135 Rodrigo et al., 2012; Domínguez-Rodrigo and García-Pérez, 2013; Domínguez-Rodrigo
136 et al., 2014c; Cobo-Sánchez et al., 2014; Organista et al., 2017, among others) was
137 favoured over the alternative use of a total station (Kluskens, 1990; Dibble et al., 1997;
138 McPherron, 2005; Enloe, 2006; Bernatchez, 2010, among others), mostly due to the
139 time-restricted conditions of the rescue excavation conducted at Marathousa 1.

140 Measurements of the bearing (azimuth) and plunge (dip) of elongated finds were
141 taken along the symmetrical longitudinal a-axis (SLA) of elongated bones (Domínguez-
142 Rodrigo and García-Pérez, 2013), lithic artefacts (Bertran and Texier, 1995) and wood
143 fragments (Macdonald and Jefferson, 1985), using the lowest endpoint of the a-axis as
144 an indicator of the vector direction.

145 Other major axes have been alternatively used with the recent application of GIS
146 techniques to retrieve orientation data from secondary source, i.e., from excavation
147 photographs, drawings or maps (Boschian and Saccà, 2010; Benito-Calvo and de la
148 Torre, 2011; de la Torre and Benito-Calvo, 2013; Walter and Trauth, 2013; García-
149 Moreno et al., 2016; Sánchez-Romero et al., 2016). However, the experimental works
150 of Domínguez-Rodrigo and García-Pérez (2013) and Domínguez-Rodrigo et al. (2014c)

151 showed that the SLA, defined as the major axis which symmetrically divide the bone,
152 is more accurate in estimating the flow direction, regardless of bone shape. This a-axis
153 is widely used in taphonomic studies (Toots, 1965; Voorhies, 1969; Eberth et al., 2007;
154 Domínguez-Rodrigo et al., 2012, 2014a; Aramendi et al., 2017, among others) for de-
155 termining the preferential orientation of anisotropic assemblages. The a-axis or major
156 axis of the artefact, measured as the long diameter of the triaxial ellipsoid that approx-
157 imates the particle shape (Krumbein, 1941), is as well used in studies which employ a
158 sedimentological approach to archaeological fabric (Bertran and Texier, 1995; Bertran
159 et al., 1997; Lenoble and Bertran, 2004; Benito-Calvo et al., 2009, among others).

160 The present study focuses on the excavated stratigraphic units in which most of the
161 archaeological and palaeontological remains were recovered in both excavation areas,
162 namely in UA3c and UA4 in Area A, and UB4c and UB5a in Area B. From the total,
163 subset samples of material were used for each specific spatial analysis. For the fabric
164 analysis we included material collected until 2016. For the vertical distribution and
165 point pattern analyses, the region of investigation was limited to the squares excavated
166 from 2013 until 2015, 25 and 29 square meters respectively in each area (Fig. 2).

167 The analyses were performed in R statistical software (R Core Team, 2017). In
168 order to make this research reproducible (Marwick, 2017; Marwick et al., 2017), a
169 repository containing a compendium of data, source code and text is open licensed and
170 available at the DOI: [10.5281/zenodo.822272](https://doi.org/10.5281/zenodo.822272)

171 *2.1. Fabric analysis*

172 The taphonomic study of the orientation pattern of elongated sedimentary particles,
173 including bones and artefacts, first addressed by Voorhies (1969); Isaac (1967); Bar-
174 Yosef and Tchernov (1972); Schick (1986), more recently led to a noteworthy develop-
175 ment of methods and propagation of applications in Palaeolithic site formation studies
176 (Bertran and Texier, 1995; Bertran et al., 1997; Lenoble and Bertran, 2004; Lenoble
177 et al., 2008; McPherron, 2005; Benito-Calvo et al., 2009, 2011; Benito-Calvo and de la
178 Torre, 2011; Bernatchez, 2010; Boschian and Saccà, 2010; Domínguez-Rodrigo et al.,
179 2012; Domínguez-Rodrigo and García-Pérez, 2013; Domínguez-Rodrigo et al., 2014c;
180 de la Torre and Benito-Calvo, 2013; Walter and Trauth, 2013; García-Moreno et al.,
181 2016; Sánchez-Romero et al., 2016, among others).

182 Fabric analysis can provide valuable insight into site formation and taphonomic
183 processes, allowing discrimination between different orientation patterns (isotropic,
184 linear or planar) possibly associated with a range of sedimentary processes. Whereas
185 water-flow deposits are generally characterised by relatively good sorting and preferred
186 orientation of clasts parallel, or normal to the flow direction (linear fabric) (Petraglia
187 and Potts, 1994); debris-flow deposits mostly exhibit massive, poorly bedded mixtures
188 of unsorted sediments and random orientation of clasts (isotropic fabric), except at the
189 flow margins where linear fabric may occur (Pierson, 2005). On the other hand, undis-
190 turbed archaeological sites, as well as experimental assemblages, have been observed
191 to have planar fabric (Bertran et al., 1997; Lenoble and Bertran, 2004). Nevertheless,
192 grey zones exist between depositional processes, so that an unequivocal discrimination
193 based only on fabric observations is often not possible, and other taphonomic criteria
194 must also be considered (Lenoble and Bertran, 2004). As an example, while overland
195 flows (runoff) have been observed to show some degree of planar fabric (Lenoble and

[Bertran, 2004](#)), anisotropy without significant transport can be caused in a lacustrine floodplain by low-energy processes such as lake transgression and regression, as well as water-sheet flows formed during rainy seasons ([Cobo-Sánchez et al., 2014](#)).

At the margin of a lacustrine environment, relatively close to the surrounding relief, a combination of high- and low-energy processes can be expected. According to the sedimentological and micromorphological study of the Marathousa 1 site, the main find-bearing horizon is associated with hyperconcentrated flows ([Karkanas et al., this issue](#)). Hyperconcentrated flows are intermediate states, defined by sediment concentration, in the continuum between sub-aerial water flows and debris flows. [Benvenuti and Martini \(2002\)](#) reported that, when a turbulent hyperconcentrated flow expands over a surface - as in the case of Marathousa 1 - a two-phase flow may develop, with a more concentrated, coarser grained bottom flow-layer (traction carpet) moving slower than the upper turbulent flow-layer carrying wash-load and suspended load. Resultant deposit may exhibit diagnostic inverse grading, or a continuously aggrading bed. Parallel or normal orientation of the clasts to the flow direction can be observed ([Benvenuti and Martini, 2002](#)). A simulation model also showed that linear fabric can develop in mud flows. However, after deposition, settling of the clasts may affect the fabric to some extent, depending on the viscosity of the mud flow ([Lindsay, 1968](#)).

As part of our three-prong spatial analytic approach, we conducted comparative fabric analysis with the aim to investigate the dynamics of the depositional processes at Marathousa 1.

Since fabric strength has been found to be positively correlated with the shape and size of the clast, for the fabric analysis we subset samples of remains with length ≥ 2 cm and elongation index (the ratio length/width) $I_e \geq 1.6$ ([Lenoble and Bertran, 2004](#)). The samples are listed in Table 1 and include mostly wood fragments and faunal remains from the four stratigraphic units under investigation. Bones have been found to readily react to water flow and show very early anisotropic patterns ([Domínguez-Rodrigo et al., 2014c](#)). Flume experiments showed that wood fragments as well tend to align parallel to the current direction ([Macdonald and Jefferson, 1985](#)). No distinction of skeletal elements was made, both due to the high fragmentation rate of faunal remains in Area B, and because recent experiments showed a similar orientation pattern for different bone shapes ([Domínguez-Rodrigo et al., 2012; Domínguez-Rodrigo and García-Pérez, 2013](#)).

The sample of bones belonging to the individual of *P. antiquus* from Area A was analysed separately and included the humerus, ulna, femur and tibia; the atlas, axis and other 16 complete vertebrae or vertebral fragments; 29 complete ribs or rib fragments; 2 calcanea; 4 metatarsals/metacarpals; the pyramidal; the trapezoid and the pelvis. The sample from UB5a was too small (only 7 observations) and was therefore excluded. In order to assess the reliability of the orientation data recorded using the clock method, we separately analysed two sub-samples from unit UB4c, selected from a set of finds recorded using both methods. All the sampled observations are representative of the whole study area.

Rose diagrams and uniformity tests, such as Rayleigh, Kuiper, Watson and Rao tests ([Jammalamadaka et al., 2001](#)), were used to visualise and evaluate circular isotropy in the sample distribution. The Rayleigh test is used to assess the significance of the sample mean resultant length (\bar{R}), assuming that the distribution is unimodal and not

Table 1: List of sampled observations for the fabric analysis.

Sample	<i>n</i>	Type		
		Fauna	Wood	Lithic
UA3c	49	23	25	1
UA4	38	8	30	-
<i>P. antiquus</i>	63			
UB4c	38	30	1	7

242 bi- or plurimodal. The \bar{R} ranges from 0 to 1: values close to 1 indicate that the data are
 243 closely clustered around the mean direction; when the data are evenly spread \bar{R} has a
 244 value close to 0. A *p* – *value* lower than 0.05 rejects the hypothesis of uniformity with
 245 a 95% confidence interval. Kuiper, Watson and Rao are omnibus tests used to detect
 246 multimodal departures from circular uniformity. The test results are evaluated against
 247 critical values: a result higher than the critical value rejects with confidence the null
 248 hypothesis.

249 Randomness testing of three-dimensional data was conducted with the Woodcock
 250 S_1/S_3 test (Woodcock and Naylor, 1983). Considering both the plunge and bearing
 251 of the oriented items, this method, based on three ordered eigenvalues (S_1, S_2, S_3), is
 252 able to discriminate the shape and strength of the distributions. The shape parameter
 253 $K = \frac{\ln(S_1/S_2)}{\ln(S_2/S_3)}$ ranges from zero (uni-axial girdles) to infinite (uni-axial clusters). The
 254 parameter $C = \ln(S_1/S_3)$ expresses the strength of the preferential orientation, and
 255 its significance is evaluated against critical values from simulated random samples of
 256 different sizes. A perfect random uniform distribution would have $C = 0$ and $K = 1$.

257 The Benn diagram (Benn, 1994) adds to the Woodcock test an isotropy ($IS =$
 258 S_3/S_1) and an elongation ($ES = 1 - (S_2/S_1)$) index. Like the former method, it is
 259 able to differentiate between linear (cluster), planar (girdle) or isotropic distributions.
 260 There are no published raw data from actualistic studies on hyperconcentrated flows or
 261 other depositional processes affecting the orientation of bones and artefacts deposited
 262 on lacustrine floodplains (but see Morton (2004) and Cobo-Sánchez et al. (2014) as
 263 pioneer studies on this subject). However, we included in the Benn diagram relevant
 264 references to published results from observation of fabrics in modern subaerial slope
 265 deposits, i.e., debris flow and runoff (Bertran et al., 1997; Lenoble and Bertran, 2004).

266 2.2. Vertical distribution

267 The vertical distribution of materials has been long investigated with the aim of
 268 identifying cultural levels, by visually interpreting cross-sectional plots. However,
 269 recent advances in GIS techniques allow to inspect at higher resolution the three-
 270 dimensional distributions of archaeological remains (McPherron et al., 2005; Anderson
 271 and Burke, 2008, among others).

272 In analysing the vertical dispersion of material at Marathousa 1, we provisionally
 273 assume that a general concentration of unsorted lithic artefacts and faunal remains in
 274 the proximity of the erosional surfaces would support an autochthonous origin of the
 275 assemblages; whereas a homogeneous vertical distribution of remains from the UA3c
 276 and UB4c units would suggest an allochthonous origin, significant transport and subse-

Table 2: List of sampled observations for the vertical distribution and point pattern analyses.

Sample	<i>n</i>	Lithic class					Faunal class			
		Debris/chip	Flake	Bone flake	Tool	Core	Indet.	Bone	Tooth	Microfauna
UA3c	279	46	2	-	1	-	1	171	14	44
UA4	61	3	1	-	-	-	-	45	4	8
UB4c	1243	753	154	1	34	6	2	246	28	19
UB5a	101	50	12	-	3	-	-	30	3	3

quent re-deposition of the material. Indeed, massive process such as hyperconcentrated flows, have high erosional power and rather chaotic structure, which may result in inverse or normal grading ([Benvenuti and Martini, 2002](#)).

In order to estimate the degree of vertical dispersion while controlling for the size of the archaeological material, dimensional classes were set up following typological criteria. Lithic artefacts were classified as debris/chips when smaller than a cutoff length of 15 mm ([Tourloukis et al., this issue](#)). Other classes include flakes, tools and cores; the latter being the bigger and heavier debitage product. Table 2 summarises the sample size for each class. Lithic debris/chips constitute the larger part of the assemblage from UB4c (60%) and UB5a (49%); whereas in Area A they represent only a moderate percentage in the upper UA3c unit (16%). The very rare presence of lithic artefacts in the underlying unit UA4 is nevertheless significant. In this unit, the faunal remains are also found in much lower numbers, their number reduced to one fourth of those found in UA3c. For the point pattern analysis (see below), we used the same subset of material for both excavation areas.

For Area B, the material recovered from the water-screening was randomly provenanced according to the 5 cm depth of the excavated spit and the coordinates of the 50x50 cm quadrant of the excavation square. Following the same excavation protocol, the same procedure was applied for the water-screened material of Area A, which was randomly provenanced according to 3D-coordinates of the 1x1 m excavation square and 10 cm spit.

Since the merely projection of points to virtual profiles is not a suitable method of analysis in presence of erosional, and thus uneven, geological contacts - such as those at Marathousa 1, ordinary Kriging interpolation of the recorded points of contact between the UA3c/UA4 and the UB4c/UB5a stratigraphic units were used to reconstruct the UA3c/4 and UB4c/5a erosional surfaces (Fig. 5a,b). In geostatistics, Kriging is a method of interpolation which, from a modelled function of spatial autocorrelation between known points (e.g., recorded elevations), calculates values of unknown points (e.g., predicted elevations). Thus, in order to address our specific objective, i.e., to quantify and analyse the vertical distribution of the archaeological and palaeontological material, we measured the minimum orthogonal distance (*d*) of each specimen to the interpolated erosional surface (Fig. 5c). For the units above and below this surface (i.e., UB4c and UB5a), the relative distribution of lithic classes and faunal remains was informally tested by means of kernel density estimations.

In Area A, the UA3c/4 erosional contact is locally sharp, but, in contrast to Area B, parts of the eroded unit UA4 are mixed with pockets of the UA3c organic-rich silty sands and intraclast-rich mud flows ([Karkanas et al., this issue](#)). However, from sparse

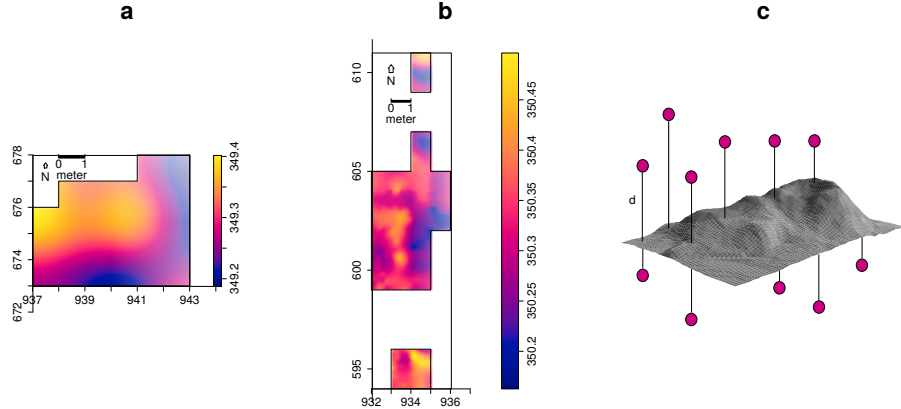


Figure 5: Ordinary Kriging interpolation of the UA3c/4 (a) and UB4c/5a (b) erosional surface; the colour scale denotes absolute elevation in m a.s.l. (c) Illustration of the method used to quantify the vertical dispersion of remains (d) with respect to the UA3c/4 (a) and UB4c/5a (b) surface.

known points of the erosional contact, the UA3c/4 surface was interpolated and the vertical dispersion of remains estimated as well. The elephant remains were excluded from this analysis, since they clearly lie horizontally at the UA3c/4 contact (Fig. 4a).

Finally, a Student's two sample t-test allowed us to compare the empirical distributions of different groups of remains for each stratigraphic unit.

2.3. Point pattern analysis

A spatial point pattern is defined as the outcome of a random spatial point process (repetitions of it would always create a different pattern). The observed patterns of the archaeological and palaeontological remains were treated as manifestations of spatial point processes, i.e., site formation processes. Point pattern analysis investigates the spatial arrangement of points with the aim of identifying spatial trends. In order to integrate the previous studies of the fabric and vertical distributions, we directed our point pattern analysis equally to the intensity of the patterns (the rate of occurrence of the recorded finds) and to the spatial interaction between different types of finds.

As the average number of random points per unit area, intensity informs about homogeneity or inhomogeneity in the distribution of events (e.g., clasts) generated by a point process (e.g., mud flow), i.e., whether the rate of occurrence is uniform or spatially varying across the study area. Intensity, usually non-parametrically evaluated by means of kernel density estimation (Diggle, 1985), was assessed for the distribution of material from the UB4c, UB5a and UA3c units. Cross-validation bandwidth, which assumes a Cox process, and edge correction were applied using the methods described in Diggle (1985).

In the presence of a covariate, it is recommended to further investigate the dependence of intensity on that explanatory variable (Baddeley et al., 2012). In order to evaluate whether variation in the density of materials was correlated to the topography

of the erosional surface, we computed a local likelihood smoothing estimate of the intensity of remains from UB4c as a function of the UB4c/5a surface elevation model. Formal tests enabled us to assess the evidence of that dependence and to quantify the strength of the covariate. The Kolmogorov-Smirnov test of CSR (Complete Spatial Randomness) and Berman's Z_2 statistics were used to test the strength of evidence for a covariate effect. The Receiver Operating Characteristic (ROC) plot, and the area under the ROC curve (AUC), closely related to Berman's Z_2 test, measure the magnitude of the covariate effect. AUC values close to 1 or 0 indicate strong discrimination, whereas intermediate values (0.5) suggest no discrimination power.

Intensity, evaluated by means of kernel density maps, although informative and widespread in the literature, nonetheless does not provide sufficient information to reliably infer about site formation processes.

Whereas intensity is a first-order property of the point process, multiscale inter-point interaction is measured by second or higher-order moment quantities, such as the Ripley's K correlation function (Ripley, 1976, 1977) and the distance G -, F - and J -functions. Three different types of inter-point interaction are possible: random, regular or cluster. In a hypothesis-testing framework, point-wise envelopes are computed by a number of random simulations of the null hypothesis (i.e., random/Poisson distribution). Thus, values of the empirical distribution (black solid line) are plotted against the benchmark value (red dotted line) and the envelopes (grey area) which specify the critical points for a Monte Carlo test (Ripley, 1981). Regular patterns are assumed to be the result of inhibition processes, while cluster patterns are the result of attraction processes.

In order to test the spatial interaction between remains associated with the erosional event of UB4c and those associated with the underlying UB5a unit, we treated the data as a multivariate point pattern, assuming that the point patterns in UB4c and UB5a are expressions of two different stationary point processes, i.e., depositional events. We performed a cross-type pair correlation function ($g_{ij}(r)$), derivative of the multitype $K_{ij}(r)$ function, which is the expected number of points of type j lying at a distance r of a typical point of type i . The function is a multiscale measurement of the spatial dependence between types i (UB4c) and j (UB5a). Randomly shifting in 199 Monte Carlo permutations each of the two patterns, independently of each other, estimated values of $\hat{g}_{ij}(r)$ are compared to a benchmark value $g_{ij}(r) = 1$, which is consistent with independence or at least with lack of correlation between the two point processes.

In addition to the pair correlation function, the multitype nearest-neighbour $G_{ij}(r)$ function was used to estimate the cumulative distribution of the distance from a point of type i (UB4c) to the nearest point of type j (UB5a). It measures the spatial association between the two assemblages. For the cross-type G -function, the null hypothesis states that the points of type j follow a Poisson (random) distribution in addition to being independent of the points of type i .

Thus, in a randomisation technique, when the solid line of the observed distribution ($\hat{G}_{ij}(r)$ or \hat{g}_{ij}) is above or below the shaded grey area, the pattern is significantly consistent with clustering or segregation, respectively. In order to reduce the edge effect bias in estimating the correlation between points, we implemented Ripley's isotropic edge correction (Ohser, 1983; Ripley, 1988).

Complete spatial randomness and independence (CSRI) of the two point processes

Table 3: Value and p – value of circular uniformity test statistics.

Sample	mean dir.	Rayleigh		Kuiper		Watson		Rao	
		R	p	V _n	p	U ²	p	U	p
UA3c	77.17°	0.268	0.029	2.4698	<0.01	0.2967	<0.01	271.8367	<0.001
UA4	35.79°	0.386	0.003	2.5656	<0.01	0.3437	<0.01	246.3158	<0.001
<i>P. antiquus</i>	54.64°	0.489	2.775e-07	3.4811	<0.01	0.906	<0.01	291.4286	<0.001
UB4c (clock)	91.66°	0.276	0.054	1.8963	0.01< p <0.025	0.1937	0.025< p <0.05	255.7895	<0.001
UB4c (compass)	151.17°	0.243	0.106	1.3944	>0.15	0.1268	>0.10	128.5263	>0.10

(UB4c and UB5a) would support an allochthonous origin hypothesis for the assemblage recovered from the UB4c unit. According to the allochthonous model, the massive, chaotic UB4c flow event randomly re-elaborated the material entrained in it, independently from the material deposited in UB5a. On the other hand, positive or negative association can be interpreted as expressions of different autochthonous processes.

As for the three-dimensional distribution of the lithic artefacts in Area A, and their spatial association with the partial skeleton of the *P. antiquus*, we applied three-dimensional univariate and bivariate second-order functions. A rectangular box of 20 square meters and 80 cm vertical extent was selected for the analyses (green outline in Fig. 11a). Assuming homogeneity, the univariate pair correlation function ($g_3(r)$) was estimated for the pattern of all the artefacts (mostly debris/chips) from UA3c and UA4.

In the specific context of the site, complete spatial randomness (CSR) would suggest that the pattern most probably is the result of a random distribution process, such as a high energy mass movement, thus supporting an allochthonous model of deposition. On the other hand, spatial aggregation would support a primary origin of the assemblage. Nevertheless, topography and natural obstructions may generate spatial clustering as well.

In support to the pair correlation function, the cross-type nearest-neighbour function has been applied in order to compute, for each artefact recovered from the UA3c and UA4 units, the nearest point of the three-dimensional clouds of points associated with the elephant skeleton. A prevalence of short distances would indicate aggregation of the lithic artefacts around the mass of the elephant; whereas a uniform or symmetric distribution would support the action of random independent processes.

3. Results

3.1. Fabric analysis

The rose diagrams in Fig. 6 visualise the circular distributions of the examined specimens. Overall, the UA4 sample and the sample of elephant bones show unimodal distributions with predominant peaks in the NE quadrant; while the ones from units UA3c and UB4c suggest multimodal distributions. Specifically, the UA4 sample distribution (Fig. 6b) spreads largely in the NE quadrant. Similarly, the circular distribution of the elephant sample (Fig. 6c), mainly lying in UA4, resembles the former distribution: it is skewed to the SW and concentrated in the NE quadrant. On the other hand, the UA3c sample (Fig. 6a) shows a bimodal distribution with two peaks to the E and NE, and the two samples from Area B (Fig. 6d,e) suggest a different multimodal scenario uniformly distributed.

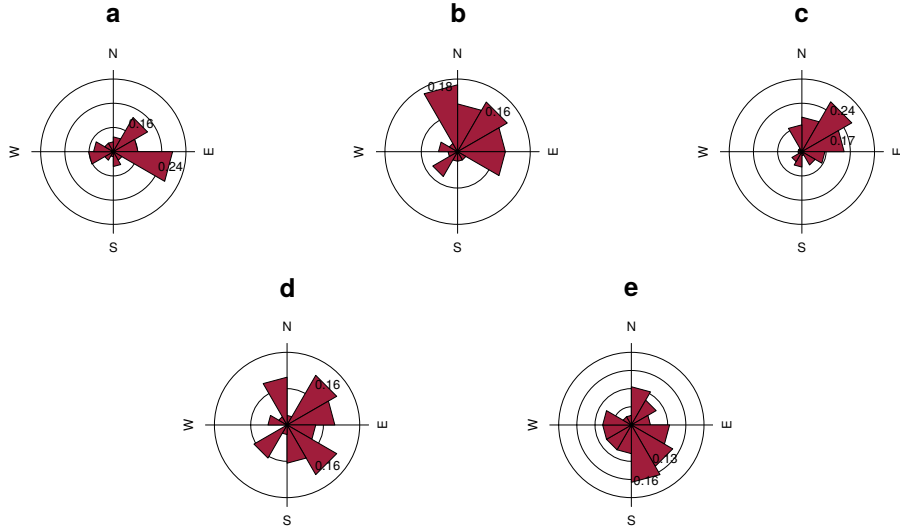


Figure 6: Rose diagrams showing the bearing patterns of samples from UA3c (a), UA4 (b), the elephant carcass (c) and UB4c (d: clock method, e: compass method).

Table 3 summarises the results of the circular uniformity tests. With regard to the UA3c sample, the Rayleigh test ($p-value = 0.03$) rejected the null hypothesis of circular uniformity. The mean resultant length ($\bar{R} = 0.27$) and the mean direction of 77° are thus significant, assuming the distribution is unimodal. However, the rose diagram (Fig. 6a) showed a bimodal distribution. The Kuiper, Watson and Rao omnibus tests, more powerful than the Rayleigh test in detecting multimodal deviation from uniformity, also rejected the null hypothesis of uniformity, therefore suggesting significant anisotropy in the distribution.

For the UA4 sample and the subset of elephant bones, all the uniformity tests agreed in rejecting the null hypothesis in favour of a preferentially oriented distribution. The elephant sample, with respect to the other, showed significantly higher test results, thus stronger anisotropy. As suggested by the rose diagrams (Fig. 6c), this sample has a mean direction towards the NE (55°) and relatively low circular variance (29°).

The UB4c sub-samples had discordant test results when considering the omnibus statistics. However, according to the Rayleigh test, the mean resultant lengths (\bar{R}) and the mean directions were not significant for both sub-samples of measurements: $p-values > 0.05$ failed to reject the null hypothesis of isotropy with 95% confidence interval. This result is well confirmed by the Kuiper, Watson and Rao tests for the sub-sample of measurements recorded using the compass. Conversely, the omnibus tests failed to reject the hypothesis of uniformity for the other sub-sample of measurements recorded with the clock method. The rose diagram (Fig. 6d) suggested for the latter distribution strong multimodality, with uniformly spread peaks. The contrasting results obtained for the UB4c sub-samples are most probably due to the shape of those distributions. Indeed, the clock system, being less accurate, tends to produce a less

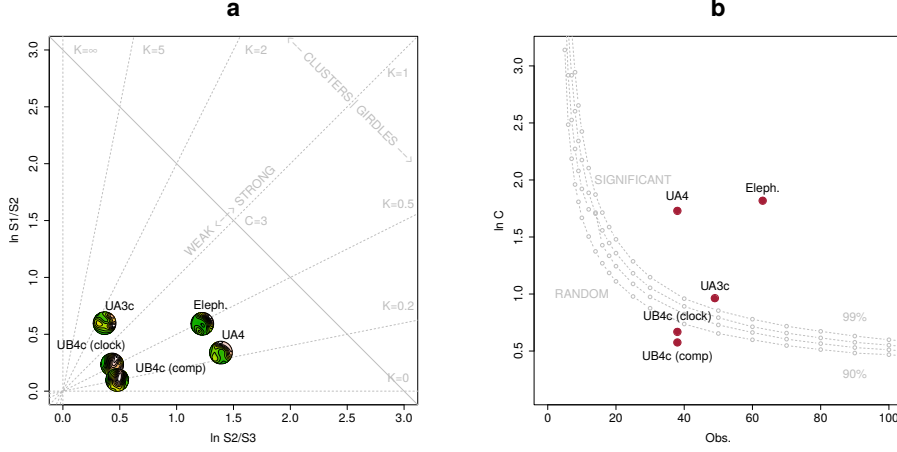


Figure 7: Woodcock's eigenvalues ratio graph (a) and plot of the Monte-Carlo critical S_1/S_3 test values, for varying sample sizes and confidence levels (b), modified from [Woodcock and Naylor \(1983\)](#).

444 dense distribution, more subject to show a multimodal shape when the distribution is
 445 actually uniform.

446 The Woodcock eigenvalues ratio graph (Fig. 7a) presents the shape (K) and strength
 447 (C) of the distributions. Fig. 7b plots confidence levels of Monte-Carlo critical C val-
 448 ues, varying for sample sizes. The two sub-samples from Area B nearly overlapped,
 449 thus suggesting reliability of the orientation measurements collected using the clock
 450 system, although of low accuracy. The two sub-samples, together with the UA3c sam-
 451 ple, having low C values, plotted close to the origin of the ratio graph. Therefore, they
 452 indicate weak preferential orientation (UA3c) and significant randomness (UB4c). On
 453 the other hand, the UA4 and the elephant samples, with higher C values, showed a
 454 stronger and significant tendency to orient preferentially. The shape parameter K of
 455 the samples varied from $K = 0.25$ for the UB4c sample measured with the compass,
 456 to $K = 0.66$ for the one measured with the clock, to $K = 0.48$ for the elephant sample.
 457 Overall, all the samples, except the UA3c one ($K = 1.63$), plotted below the average
 458 shape value ($K = 1$) between girdles and clusters distributions.

459 The Benn diagram (Fig. 8) resembles the Woodcock ratio graph (Fig. 7a). The
 460 samples from units UB4c and UA3c clearly plotted at a distance from the UA4 and
 461 the elephant samples. The UB4c samples plotted in the upper corner of the ternary
 462 graph, with the UB4c sub-sample of measurements taken with the compass exhibiting
 463 more isotropy. The UA3c sample, with an elongation index similar to the elephant
 464 sample, but higher isotropic index, plotted towards the centre. Compared to the ranges
 465 of fabrics recorded for modern natural processes (debris flow and runoff), the fabric
 466 from the UA3c and UB4c units plotted well inside the cluster of debris flows, with the
 467 UB4c (comp) sample suggesting even more random orientations. On the other hand,
 468 the sample of elephant remains, which lie mostly on UA4 and are covered by UA3c,
 469 plotted significantly close to the sample from unit UA4. They both presented the lowest
 470 isotropy index (IS), but not high elongation index (EL). Thus, they plotted in the

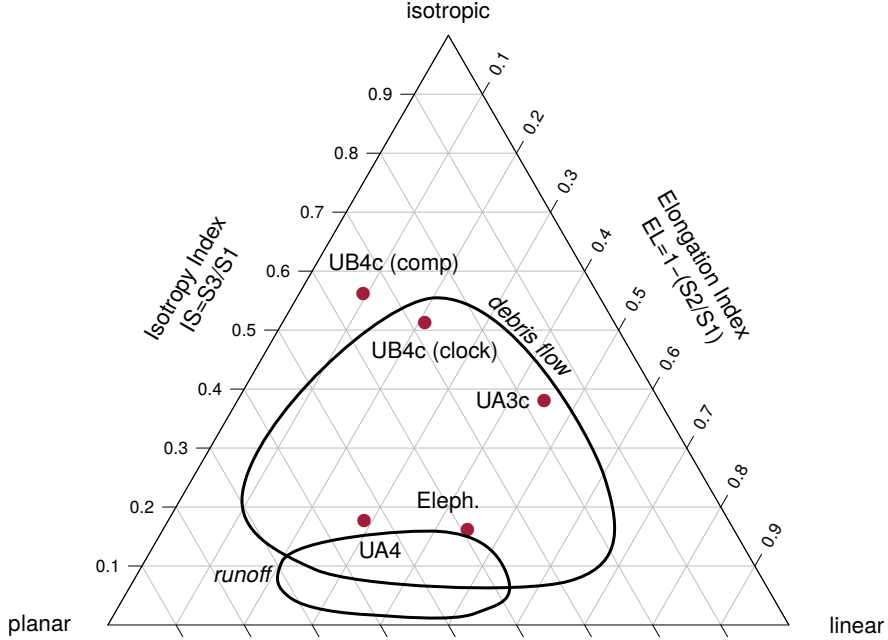


Figure 8: Benn's diagram. Fabric ranges of natural processes modified from [Lenoble and Bertran \(2004\)](#).

average between linear and planar orientations, at the margins of the range of runoff processes. Yet they still plotted within the cluster of debris flows fabrics. Moreover, as suggested also by the uniformity tests (Tab. 3), the elephant sample showed a more linear attitude with respect to the UA4 sample.

3.2. Vertical distribution

Fig. 9 compares the vertical distribution of the finds from units UA3c and UA4, by means of empirical density functions of the minimum distances (d) from each specimen to the UA3c/4 erosional contact (Fig. 5a). Three lithic artefacts (two flakes and one tool) from the UA3c unit, not included in Fig. 9, plotted within 15 cm from the interpolated surface. Only one flake has been found in the lower UA4, at about 17 cm from the UA3c/4 contact, together with three chips. Despite the scarcity ofdebitage products in this area, waste products (debris/chip) are relatively well represented (16% of the UA3c sample). Their vertical dispersion approximated a normal distribution ($\mu = 0.24$, $\sigma = 0.15$): the Kolmogorov-Smirnov and Shapiro tests failed to rejected the null hypothesis of normality ($p - value = 0.83$ and 0.075 , respectively). Notably, the distributions of the faunal remains from the same unit UA3c were all right skewed, with means (μ) about 20 cm above the UA3c/4 contact. Nevertheless, the Welch two sample t-test ($p - value = 0.61$) failed to reject the null hypothesis that the lithic and faunal sample means are equal. The total distribution of remains from unit UA3c showed a unimodal distribution, skewed to the right, with mode in the proximity of the UA3c/4

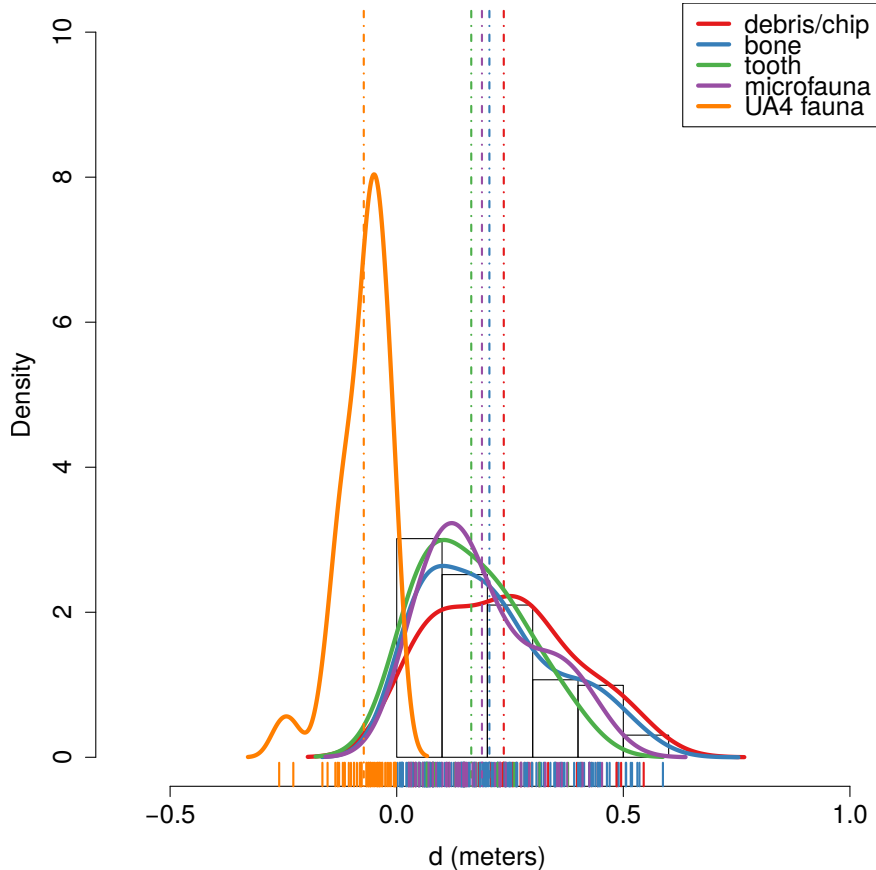


Figure 9: Empirical density functions of minimum orthogonal distances (d) to the UA3c/4 surface. The histogram represents the total distribution of remains from UA3c; dashed lines indicate mean values.

surface. Similarly, the vertical distribution of faunal remains recovered from unit UA4 concentrate in the first 10 cm below surface. The density functions altogether clearly confirmed one of the main observations assessed during excavation, namely that, with the elephant remains lying at the UA3c/4 contact and covered by unit UA3c, most of the faunal and lithic material were recovered from unit UA3c (Fig. 2) and predominantly in the proximity of the UA3c/4 contact (Fig. 9).

Fig. 10 shows the empirical density functions of the minimum distances from each specimen from Area B to the UB4c/5a erosional contact (Fig. 5b). The combined distribution of any type of find from the UB5a unit (Fig. 10a) skewed to the left with a short tail (up to -0.3 m). The mode, between 5 and 10 cm below the roof of UB5a, indicates a general concentration of material very close to the contact of this unit with the overlying UB4c, in accordance with the mean distribution of the different classes of remains. Although the majority of both the lithic and faunal assemblages were found

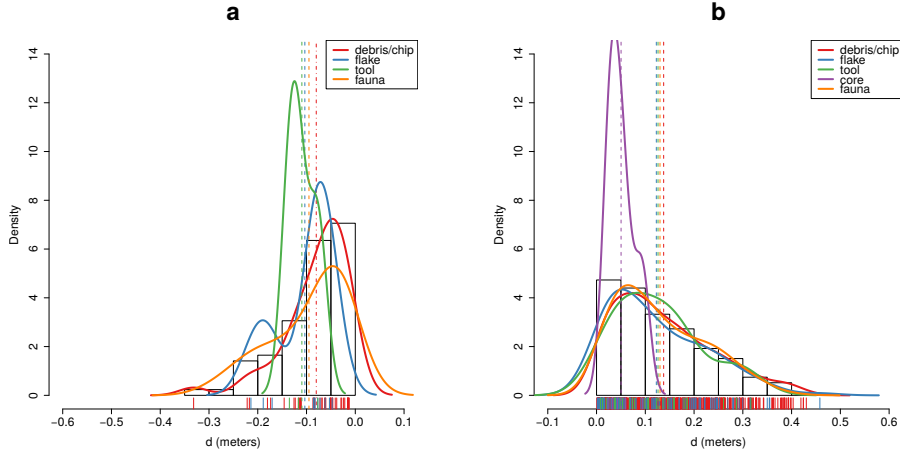


Figure 10: Empirical density functions of minimum orthogonal distances (d) to the UB4c/5a surface. The histogram represents the total distribution of remains from UB5a (a) and UB4c (b); dashed lines indicate mean values.

in the uppermost 15 cm of UB5a, few debris/chips and bone fragments occur lower in the sequence, yet no more than 30 cm below the roof of this unit. Very few flakes, three tools and no cores have been found in this unit. As a whole, the lithic assemblage from UB5a, mostly composed by debris/chips, is only 7% of the most conspicuous assemblage from UB4c.

The global distribution of unit UB4c was right skewed (up to almost 0.6 m) and centred at about 5 cm above the contact with the underlying unit UB5a (Fig. 10b). Almost 30% of the sample fell exactly at the erosional contact that separates UB4c from UB5a. The density estimations of the lithic debris/chip, flakes, tools and faunal remains significantly overlap, whereas the distribution of the six cores shows a bimodal shape with peaks at 5 and 20 cm above the contact. Moreover, the Welch Two Sample t-test of the lithic and faunal sample means failed to reject the null hypothesis (p -value = 0.6295).

3.3. Point pattern analysis

Results of the point pattern analysis are complementary to those obtained from the analysis of the fabric and vertical distributions.

Regarding Area A, kernel density estimation and three-dimensional functions were applied in order to quantitatively depict the spatial distribution of the lithic assemblage in relation to the elephant skeleton. Fig. 11a shows the smoothing kernel intensity estimation of the faunal assemblage from the UA3c unit. Contour lines delimit the density of the lithic sample. The partial skeleton of the *P. antiquus* is superimposed on it. A preliminary visual examination of the plot suggests a homogeneous distribution of lithics (mostly debris/chips) and fossils. Spots of higher density appear to be spread around and in association with the elephant remains.

528 The univariate pair correlation function of the joined lithic assemblage from the
529 UA3c and UA4 units (Fig. 11b) suggests aggregation of finds. The estimated $\hat{g}_3(r)$
530 function (black solid line) wanders above the benchmark value (red dotted line) until
531 values of $r = 0.8$. However, for distances between 35 and 65 cm, it lies above the
532 grey envelope of significance for the null hypothesis of CSR, indicating that at those
533 distances artefacts occur significantly closer than expected in the case of random pro-
534 cesses. For values of $r > 0.8$, the function stabilises at values close to 0, suggesting
535 a Poisson distribution. The plot illustrates the random distribution of finds between
536 patches of clusters that we observe in Fig. 11a.

537 The histogram in Fig. 11c shows the density of the distances calculated from each
538 artefact to the nearest-neighbour elephant remain. A right skewed distribution, with a
539 prevalent peak at 10 cm and mean (μ) 30 cm is an indication of the relatively strong
540 aggregation of lithics around the mass of the elephant skeleton.

541 As for Area B, the analysis focused on the spatial distribution and cross-correlation
542 of the assemblages from UB4c and UB5a. Figs. 12a,b respectively show kernel density
543 estimations of the combined lithic and faunal assemblages from both the units analysed.
544 Despite the samples size difference, a first visual examination suggests the presence of
545 interesting spatial structures.

546 Regarding the UB4c unit (Fig. 12a), the high density of material concentrated
547 around the western square 934/600 suggests that the pattern could have been the re-
548 sult of an inhomogeneous, non-uniform depositional process. Visual comparison of
549 the density plot with the elevation model of the erosional contact between the UB4c
550 and UB5a units (Fig. 5b) suggests positive correlation between lower elevations (topo-
551 graphic depressions) and higher density of remains. Fig. 12c shows the results of the
552 ρ -function, which estimates the intensity of the UB4c sample assemblage as a func-
553 tion of the covariate underlying topography created by the erosional event. Within the
554 range of elevation between 350.2 and 350.4 m, the occurrence of finds is higher and
555 the intensity decreases with the rise of elevation, i.e., finds are more likely to be found
556 at lower elevations than would be expected if the intensity was constant.

557 Spatial Kolmogorov-Smirnov (KS) and Berman's Z_2 (Berman, 1986) statistics were
558 used in order to test the dependence of the UB4c pattern on the covariate erosional
559 surface. Both KS ($D = 0.11952$, $p - \text{value} = 7.772e - 16$) and Z_2 ($Z_2 = -7.8447$,
560 $p - \text{value} = 4.34e - 15$) significantly rejected the null hypothesis of CSR. Although
561 the tests suggested evidence that the intensity depends on the covariate, the effect of
562 the covariate is weak and it seems to have no discriminatory power. The ROC curve
563 and AUC statistics (0.56), which measure the strength of the covariate effect, suggest
564 that the underlying UB4c/5a topography does not completely explain the localised high
565 density of occurrence in the UB4c.

566 Relative spatial segregation seems to occur between the assemblages from UB4c
567 (Fig. 12a) and UB5a (Fig. 12b), with high density of the former distribution corre-
568 sponding to low density of the latter. The former analysis of the vertical distribu-
569 tion showed that the two assemblages occur very close to their stratigraphic contact
570 (Fig. 10). In order to further investigate the spatial interaction between the two de-
571 positional events, we applied multitype pair correlation ($g_{ij}(r)$) and nearest-neighbour
572 ($G_{ij}(r)$) functions.

573 Fig. 12d shows the estimated values of the multivariate $\hat{g}_{ij}(r)$ function against the

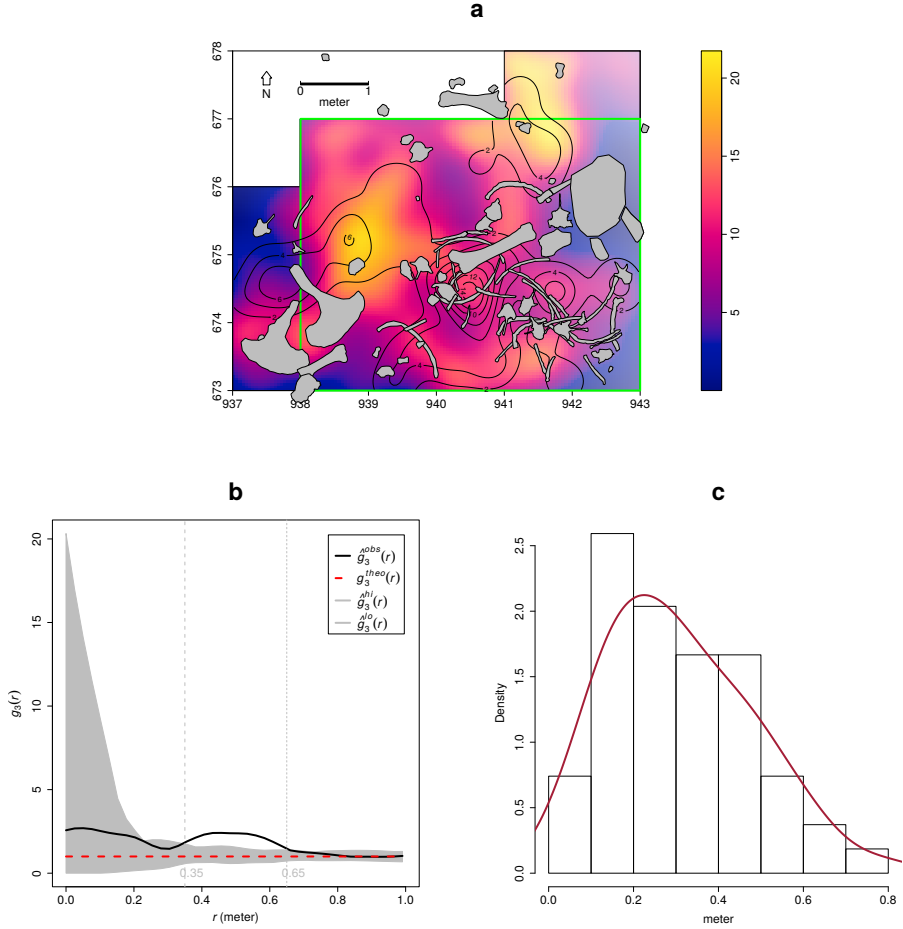


Figure 11: Kernel smoothed intensity function of the faunal assemblages from UA3c. Isolines mark the density of the lithic artefacts from UA3c (a). Pair correlation function ($g_3(r)$) of a three-dimensional pattern of lithic artefacts from UA3c and UA4. Grey envelope of 999 Monte Carlo simulations under the CSR null hypothesis (b). Three-dimensional distance from each lithic artefact from UA3c and UA4 to the nearest neighbour elephant remain (c).

envelope of the null hypothesis, obtained by randomly shifting the position of remains from the two distributions in 199 Monte Carlo simulations. For fixed values of r less than 30 cm the observed function lies below the benchmark value of independence, thus indicating segregation; but it wanders at the lower edge of the grey envelope. For fixed distances of $r > 0.3$ m the observed and theoretical lines significantly overlap. Overall, the function suggests independence of the two point processes (UB4c and UB5a) at multiple scales.

However, the estimated $\hat{G}_{ij}(r)$ function (Fig. 12c), running well below the significance grey envelope for fixed values of $r > 0.3$ m, confirms that the nearest-neighbour distances between remains from UB4c and UB5a are significantly longer than expected in the case of independent processes. Interestingly, at values of $r < 0.2$ m the observed function failed to reject the null hypothesis of Complete Spatial Randomness and Independence (CSRI).

4. Discussion

Recent excavations at the Middle Pleistocene site of Marathousa 1 have unearthed in one of the two investigated areas (Area A) a partial skeleton of a single individual of *Palaeoloxodon antiquus*, whose bones are in close anatomical association, and spatially and stratigraphically associated with lithic artefacts and other faunal remains. In Area B, 60 m to the South of Area A, we collected a much higher number of lithic artefacts (Tourloukis et al., this issue), spatially and stratigraphically associated with other faunal remains, including isolated elephant bones, cervids and carnivores among others (Konidaris et al., this issue). The two areas are stratigraphically correlated, the main fossiliferous layers (UA3c and UB4c) representing a massive depositional process, such as a hyperconcentrated flow that dumped material in a lake margin context (Karkanas et al., this issue). To date, evidence of butchering (cut-marks) has been identified on two bones of the elephant skeleton from Area A, as well on elephant and other mammal bones from Area B (Konidaris et al., this issue).

However, due to the secondary depositional nature of the main fossiliferous horizon, it is of primary importance to evaluate the degree and reliability of the spatial association of the lithic artefacts with the faunal remains, and especially with the elephant skeleton. In order to tackle our main objective, we applied a comprehensive set of spatial statistics to the distributions of the archaeological and zooarchaeological/palaeontological remains from relevant stratigraphic units of the two areas of investigation. Preliminary results of our analyses are here discussed for both areas.

4.1. Fabric analysis

The analysis of the orientation (plunge and bearing) of subsets of remains, mostly bone, wood fragments and lithic artefacts, showed different patterns for the two main find-bearing units.

In Area B, two sub-samples from the same stratigraphic unit were analysed, in order to assess the reliability of the orientation data measured with the clock system. Due to the different shapes of the distributions (Figs. 6d,e), test statistics reported contrasting results (Tab. 3). Indeed, the clock system, recording non-continuous circular data,

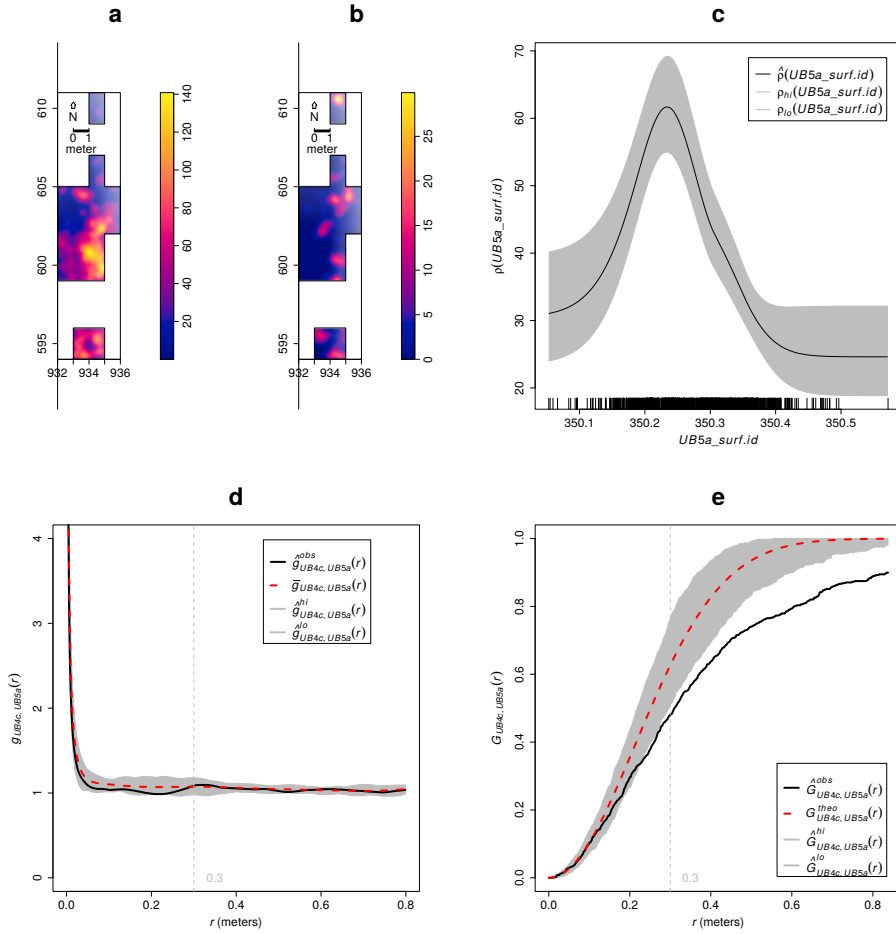


Figure 12: Kernel smoothed intensity function of the lithic and faunal assemblages from UB4c (a) and UB5a (b). Smoothing estimate of the intensity of remains from UB4c, as a function of the erosional surface UB4c/5a. Grey shading is point-wise 95% confidence bands (c). Cross-pattern pair correlation function ($g_{ij}(r)$) between the UB4c and UB5a distributions. Grey envelope of 199 Monte Carlo simulations under the independence of components null hypothesis (d). Multitype nearest-neighbour function ($G_{ij}(r)$) between the UB4c and UB5a distributions (e).

616 tends to produce a distribution more subject to show a multimodal shape when it is
617 actually uniform. However, the two sub-samples nearly overlapped when plotted in
618 the three-dimensional Woodcock (Fig. 7) and Benn (Fig. 8) diagrams, thus suggesting
619 some degree of reliability of the clock method. Nevertheless, despite minor differences
620 between the two samples, caution should be paid in analysing grouped circular data.

621 The test results (Tab. 3) for the UA4 sample and the sample of elephant remains
622 - which lie on unit UA4 and are covered by UA3c - indicated significant preferential
623 orientations towards the NE (Figs. 6b,c). As shown by the Woodcock's (Fig. 7) and the
624 Benn's diagrams (Fig. 8), these samples plotted together at a distance from the others.
625 Such convergence suggests that the elephant carcass, the other faunal remains and the
626 organic material, deposited on unit UA4, were subject to the same processes.

627 Far from the isotropic corner in the Benn's diagram these two samples from Area
628 A plotted approximately in between the linear and planar extremes, with the elephant
629 sample showing a more linear fabric. When the results published by Bertran et al.
630 (1997) and Lenoble and Bertran (2004) from observations of fabrics in modern sub-
631 aereal slope deposits were used as a reference, the two samples aggregated at the ex-
632 treme margins of runoff processes. Yet, they plotted well within the cluster of debris
633 flows and relatively distant from the linear corner.

634 Although Bertran et al. (1997) studied runoff deposits from different environments
635 (channel-lag gravels in rills, small gullies, and inter-rill surfaces on alpine slopes; and
636 faintly laminated gravel lenses on an inactive, small colluvial fan), this result is consis-
637 tent with the exposure of unit UA4 to overland water-laden processes that occurred be-
638 fore the flood event UA3c/UB4c. Notably, the erosive nature of low-energy processes
639 triggered by rain-water has been observed on lacustrine floodplains, and is associated
640 with anisotropic patterns in autochthonous assemblages (Cobo-Sánchez et al., 2014;
641 Domínguez-Rodrigo et al., 2014c; García-Moreno et al., 2016).

642 Pockets of thinly bedded organic-rich silty sands have been found mixed in UA4.
643 These sands in Area A resemble the UB5b/c sandy deposit in Area B, which is associ-
644 ated with relatively high energy fluvial flows entering the lake margins (Karkanas et al.,
645 this issue). Eventually, such relatively high energy flood (UB5b/c) would have had the
646 power to significantly reorient elements of the elephant carcass and slightly displace
647 them. However, the elephant skeleton clearly lies on top of unit UA4 and is covered by
648 UA3c (see Fig.4).

649 Moreover, unlike bones with a tubular shape (i.e., long bones), ribs and vertebrae
650 are prone to orient preferentially under high energy processes, less likely under low
651 energy processes (Domínguez-Rodrigo and García-Pérez, 2013; Domínguez-Rodrigo
652 et al., 2014c). Interestingly, whereas some of the ribs share the same preferential orien-
653 tation with the long bones, others are oriented NW/SE. However, a NW/SE orientation
654 could be consistent with a prevalent NE direction of the flow (and vice-versa), since
655 long bones could roll orthogonally to the flow direction (Voorhies, 1969). On the other
656 hand, a higher energy flood would lead to an under-representation of carpals, tarsals,
657 metapodials, phalanges, ribs and vertebrae, which are more prone - when disarticulated
658 - to be easily transported by water induced processes (Voorhies, 1969). Yet, several of
659 these bones are present and in close spatial association with the elephant cranium and
660 other skeletal elements. The presence of many of the skeletal elements with different
661 transportation properties suggests that the elephant carcass was not subjected to high

662 energy processes (and probably still articulated) before the flood event UA3c/UB4c.

663 The fabrics of the UA3c and UB4c samples, with higher isotropic index (*IS*), plotted
664 at a significant distance from the elephant sample, yet within the cluster of debris
665 flows (Fig. 8). Indeed, random distribution and orientation of clasts is expected for de-
666 bris flows, except at flow margins, where preferential orientation and clusters of clasts
667 have been observed (Pierson, 2005). However, hyperconcentrated flows, such as the
668 UA3c/UB4c flood event, which fall in between the spectrum of water and debris flows,
669 may develop parallel or normal orientation to the flow direction (Lindsay, 1968; Ben-
670 venuti and Martini, 2002). Notably, with respect to the UB4c sample, the UA3c sample
671 exhibits a higher elongation index (*ES*), similar to that of the elephant sample (Fig. 8).
672 Rose diagrams (Fig. 6) and uniformity tests (Tab. 3) also suggest similar fabrics of the
673 samples from Area A.

674 Thus, we can assume that an overland flow, namely UA3c/UB4c, is likely to have
675 slightly reworked and preferentially oriented to the NE the exposed elements of the
676 already dismembered (and probably already marginally displaced) elephant carcass,
677 which mostly preserves close anatomical associations, but not anatomical connections.

678 Although little is currently known about the spatial extension of the UA3c/UB4c
679 flow event, the different orientation patterns between the two areas could probably
680 be explained with lateral variability. Indeed, the same event could exhibit different
681 behaviours at different temporal and spatial points, giving rise to different distribution
682 patterns.

683 As suggested by Lenoble and Bertran (2004), fabric analysis is not sufficient to un-
684 equivocally discriminate processes and should therefore be integrated with the analysis
685 of other diagnostic features.

686 4.2. Vertical distribution

687 As for the vertical distribution, we assumed that mass processes, such as hypercon-
688 centrated flows, would predominantly distribute poor to very poor sorted clasts homo-
689 geneously throughout the sequence (Pierson, 2005). Diagnostic inverse grading, or a
690 continuously aggrading bed can be observed in the resultant deposits (Benvenuti and
691 Martini, 2002). A concentration of unsorted elements in the proximity of the erosional
692 surface, as well as the absence of any grading, would in turn suggest an autochthonous
693 assemblage.

694 The lithic assemblage from Area A - the combined units UA3c and UA4 ($n = 54$),
695 composed by a few debitage products and a relatively high number of debris/chips
696 and retouch waste products (Tab. 2) - plotted predominantly in the proximity of the
697 erosional surface created by the UA3c/UB4c event (Fig. 5a). The faunal remains from
698 unit UA3c resemble the distribution of the archaeological assemblage; whereas the
699 ones from the underlying unit UA4 plotted within 10 cm below the erosional contact.
700 Overall, the material recovered from unit UA3c did not show any grading and mainly
701 plotted at the bottom of the unit (Fig. 9). Thus, its vertical distribution is consistent
702 with the hypothesis of an autochthonous assemblage.

703 In Area B, two samples from units UB4c ($n = 1243$) and UB5a ($n = 101$) respec-
704 tively, were analysed (Tab. 2) for quantifying the minimum orthogonal distance of each
705 item to the modelled erosional surface (Fig. 5b).

706 The vertical distribution of lithic artefacts and fossils from unit UB4c showed a pre-
707 dominant peak right at the contact with the erosional surface. Almost 30% of this rich
708 sample plotted at a distance between 0 and 5 cm from the erosional contact; whereas
709 the rest gently skewed to the upper part of the unit, up to about 50 cm. The same distri-
710 bution was observed for all classes of remains, suggesting no size sorting and an origin
711 very close to the erosional surface (Fig. 10b).

712 The density distribution of the sample from the underlying UB5a unit (Fig. 10a)
713 globally indicates a more constrained vertical displacement of remains (within 30 cm
714 below the erosional surface). Whereas lithic artefacts and fossils mostly plot right at
715 the contact and just below it, a few debris/chips and faunal remains were found lower
716 in the sequence. No size sorting was observed, but, notably, lithic cores are absent and
717 the debris/chip distribution is wider than the distribution of the few flakes and tools.

718 Field observations of cracks in the clayey UB5a unit testify to shrinking and swelling
719 during wet and dry cycles (Karkanas et al., this issue), which suggests that vertical dis-
720 placement of some small lithics and fossil fragments at lower depths with respect to
721 the UB5a/4c contact probably resulted from clay desiccation.

722 Likewise, Lenoble and Bertran (2004) documented up to 30 cm vertical dispersion
723 and frequent vertical plunge of artefacts from the marshy silty clay of the Croix-de-
724 Canard site, sector 3. Furthermore, a recent experimental study of animal trampling
725 in water saturated substrates reported negative correlation with artefact size, signifi-
726 cant inclination and greater vertical displacement than any former work: a maximum
727 between 16 and 21 cm, with a mean of about 6 cm (Eren et al., 2010).

728 The fact that the majority of the remains from units UB4c and UB5a plotted at, or
729 very close to the contact between these two layers, the relatively high percentage of
730 lithics in both units, as well as the absence of grading, suggest autochthonous assem-
731 blages, deposited in UB5a and subsequently eroded *in situ* by the UA3c/UB4c flood
732 event.

733 4.3. Point pattern analysis

734 The autochthonous hypothesis was further explored by means of point pattern
735 analysis. According to this model, in both areas the lithic and faunal assemblages
736 were primarily deposited *in situ* and were subsequently eroded and re-deposited (*sensu*
737 Fernández-López, 1991) by the hyperconcentrated flow UA3c/UB4c. We assumed
738 that a completely random spatial distribution of the lithic artefacts and faunal remains
739 would suggest an allochthonous origin and subsequent re-elaboration (*sensu* Fernández-
740 López, 1991), with transport to the site by the action of a random massive process.
741 Nevertheless, clustering of artefacts is not necessarily evidence of human presence.
742 Aggregation or segregation patterns could be produced by a range of biotic and/or nat-
743 ural processes. Human activities, topography and physical obstructions alike could
744 trigger spatial aggregation.

745 The three-dimensional distribution of lithic artefacts from unit UA3c shows signif-
746 icant clustering for values of r between 35 and 65 cm. Lithic artefacts occur relatively
747 close to the skeletal elements of the elephant, at a distance between 20 and 50 cm at
748 most (Fig. 11). The richest cluster of about 20 lithic artefacts is located to the SW of
749 the cranium, close to the right femur and the scatter of ribs and vertebrae.

Considering the prevalent NE orientation of the elephant bones and the other faunal remains from UA4 and UA3c, it is not unlikely that a SW/NE oriented flood could have been responsible for the observed accumulation to the SW of the elephant cranium, which would have represented an important obstruction to the flow. A similar case of clustering of small remains, apparently dammed by a long elephant tusk, has also been observed at Castel di Guido (Italy) by [Boschian and Saccà \(2010\)](#). Secondary deposition by low-energy flows and clustering of artefacts and bones blocked by an aurochs carcass have been as well documented at the site of 'Ein Qashish (Israel) ([Hovers et al., 2014](#)).

However, the pair correlation function (Fig. 9b) suggests significant clustering of lithic artefacts at relatively small scale: a pattern less likely to be produced by a large scale massive process such as a hyperconcentrated flow. Moreover, clusters of lithic artefacts occur as well in areas with lower densities of elephant bones.

Small scale clustering; proximity to the elephant remains and the erosional surface; absence of spatial size sorting and, on the contrary, the presence of a relatively high number of lithic debris/chips associated with some flakes, tools and a rich faunal assemblage; close anatomical spatial association of the elephant skeletal elements, slightly displaced and preferentially oriented: altogether these lines of evidence support the hypothesis of an autochthonous deposition, subject to localised minor reworking.

A similar pattern can be observed in Area B, where an initial set of spatial statistics confirmed that the inhomogeneous density of remains from unit UB4c (Fig. 12a) is not completely explained by the covariate effect of the underlying complex topography created by the erosional event UA3c/UB4c (Fig. 5b).

Thus, we explored the relative spatial interaction between the UB4c and the underlying UB5a samples. We assumed that complete spatial randomness of the two independent depositional processes would occur in case of an allochthonous origin and transportation of the UB4c assemblage. The hypothesis of an autochthonous original deposition of the faunal and lithic assemblages on the UB5a unit, subsequently eroded *in situ* by a relatively high energy flood (UB4c), was tested by cross-pattern spatial correlation functions (Figs. 12d,e). Whereas the two samples are vertically adjacent to the erosional surface (Fig. 10), on the horizontal plane they are both more segregated than expected for a random distribution.

Conversely, the extraordinary preservation and number of mint to sharp, unsorted lithic artefacts from the UB4c unit; their density, positively correlated to the topography, and significantly segregated from the underlying distribution of remains; the vertical proximity of both assemblages from UB4c and UB5a to the erosional surface; as well as the random orientation pattern of the former, suggest that significant displacement of materials due to the erosional event can be excluded.

The faunal and lithic assemblages from unit UB4c therefore most likely derived from the local erosion of exposed mudflat areas (unit UB5a) and have been slightly redistributed by the same flood event that capped the elephant in Area A.

Further evidence that the recovered assemblage has not undergone substantial reworking and has retained its original characteristics would come from the refitting analysis, currently in progress. To date, 4 bone refits have been found in Area B: three from unit UB4c, respectively at 4.77, 0.05 and 0.01 m distance; and one between two mammal bone fragments from units UB4c and UB5a, at a very short distance (0.09 m).

796 Interestingly, one of the elements of the most distant refit (a *Dama* sp. mandibular
797 fragment) shows traces of carnivore gnawing ([Konidaris et al., this issue](#)).

798 In conclusion, multiple lines of evidence reject an allochthonous hypothesis of de-
799 position in favour of an autochthonous model. The erosional event UA3c/UB4c repre-
800 sents an *en masse* depositional process, i.e. a hyperconcentrated flow, in the continuum
801 between water and debris flow, which would have locally reworked at a small scale
802 the already exposed or slightly buried and spatially associated lithic and faunal assem-
803 blages.

804 Although the UA3c/UB4c process represents a snapshot of a relatively short time-
805 frame, high resolution inferences about the use of space by human groups, in terms
806 of knapping episodes and butchering activities, are unreliable in light of the current
807 information.

808 The spatial pattern observed at the site is indeed the result of the last episode in a
809 palimpsest of spatial processes. Whereas the erosional event represented by the hyper-
810 concentrated flow UA3c/UB4c caps the fossiliferous horizon and preserves the record,
811 little is known about the underlying, eroded 'occupational' surface.

812 However, whereas hunting or scavenging in the Lower Palaeolithic is still an un-
813 solved matter of debate, considering the rate of bone fragmentation, the density of lithic
814 debris/chips, the number of processed bones and their spatial density and association, it
815 is likely that the assemblage represents a complex palimpsest of locally repeated events
816 of hunting/scavenging and exploitation of lake shore resources.

817 More data from high resolution excavations in the coming years will allow us to
818 refine the coarse-grained spatio-temporal resolution of our inferences about past human
819 behaviour at Marathousa 1.

820 5. Conclusions

821 At the Middle Pleistocene open-air site of Marathousa 1, a partial skeleton of a
822 single individual of *Palaeoloxodon antiquus* was recovered in stratigraphic association
823 with a rich and consistent lithic assemblage and other vertebrate remains. Cut-marks
824 and percussion marks have been identified on the elephant and other mammal bones ex-
825 cavated at the site. The main find-bearing horizon represents a secondary depositional
826 process in a lake margin context.

827 Understanding the site formation processes is of primary importance in order to
828 reliably infer hominin exploitation of the elephant carcass and other animals. To meet
829 this aim, we applied a comprehensive set of multivariate and multiscale spatial analyses
830 in a taphonomic framework.

831 Results from the fabric, vertical distribution and point pattern analyses are consis-
832 tent with a relatively high-energy erosional process slightly reworking at a small scale
833 an exposed (or slightly buried) and consistent scatter of lithic artefacts and faunal re-
834 mains. These results are in agreement with preliminary taphonomic observations of the
835 lithic artefacts ([Tourloukis et al., this issue](#)) and the faunal remains ([Konidaris et al.,](#)
836 [this issue](#)), which also indicate minor weathering and transportation. Our analyses
837 show that multiple lines of evidence support an autochthonous origin of the lithic and
838 faunal assemblages, subject to minor post-depositional reworking.

839 **Acknowledgements**

840 This research is supported by the European Research Council (ERC StG PaGE
841 283503) awarded to K. Harvati. We are grateful to the Municipality of Megalopolis,
842 the authorities of the Region of Peloponnese, and the Greek Public Power corpora-
843 tion (ΔΕΗ) for their support. We also thank Julian Bega and all the participants in the
844 PaGE survey and excavation campaigns in Megalopolis for their indispensable coop-
845 eration. We are grateful to the editors and two anonymous reviewers for their critical
846 discussions and many constructive comments that helped to improve this manuscript.

847 **References**

- 848 Anderson, K. L., Burke, A., 2008. Refining the definition of cultural levels at Karabi
849 Tamchin: a quantitative approach to vertical intra-site spatial analysis. *Journal of*
850 *Archaeological Science* 35 (8), 2274–2285.
- 851 Aramendi, J., Uribelarrea, D., Arriaza, M. C., Arráiz, H., Barboni, D., Yravedra, J.,
852 Ortega, M. C., Gidna, A., Mabulla, A., Baquedano, E., Domínguez-Rodrigo, M.,
853 2017. The paleoecology and taphonomy of AMK (Bed I, Olduvai Gorge) and its
854 contributions to the understanding of the “Zinj” paleolandscape. *Palaeogeography,*
855 *Palaeoclimatology, Palaeoecology* (in press).
- 856 Baddeley, A., Chang, Y.-M., Song, Y., Turner, R., 2012. Nonparametric estimation of
857 the dependence of a point process on spatial covariates. *Statistics and Its Interface*
858 5 (2), 221–236.
- 859 Bailey, G., 2007. Time perspectives, palimpsests and the archaeology of time. *Journal*
860 *of Anthropological Archaeology* 26 (2), 198–223.
- 861 Bar-Yosef, O., Tchernov, E., 1972. On the palaeo-ecological history of the site of Ubei-
862 diya. Vol. 35. Israel Academy of Sciences and Humanities, Jerusalem.
- 863 Bargalló, A., Gabucio, M. J., Rivals, F., 2016. Puzzling out a palimpsest: Testing an
864 interdisciplinary study in level O of Abric Romaní. *Quaternary International* 417,
865 51–65.
- 866 Benito-Calvo, A., de la Torre, I., 2011. Analysis of orientation patterns in Olduvai
867 Bed I assemblages using GIS techniques: Implications for site formation processes.
868 *Journal of Human Evolution* 61 (1), 50–60.
- 869 Benito-Calvo, A., Martínez-Moreno, J., Mora, R., Roy, M., Roda, X., 2011. Trampling
870 experiments at Cova Gran de Santa Linya, Pre-Pyrenees, Spain: their relevance for
871 archaeological fabrics of the Upper–Middle Paleolithic assemblages. *Journal of Ar-
872 chaeological Science* 38 (12), 3652–3661.
- 873 Benito-Calvo, A., Martínez-Moreno, J., Pardo, J. F. J., de la Torre, I., Torcal, R. M.,
874 2009. Sedimentological and archaeological fabrics in Palaeolithic levels of the
875 South-Eastern Pyrenees: Cova Gran and Roca del Bous Sites (Lleida, Spain). *Jour-*
876 *nal of Archaeological Science* 36 (11), 2566–2577.

- 877 Benn, D., 1994. Fabric shape and the interpretation of sedimentary fabric data. *Journal*
878 of *Sedimentary Research* 64 (4a), 910–915.
- 879 Benvenuti, M., Martini, I. P., 2002. Analysis of terrestrial hyperconcentrated flows and
880 their deposit. In: Martini, I. P., Baker, V. R., Garzón, G. (Eds.), *Flood and Megaflood*
881 *Processes and Deposits*. Vol. 32 of *Special Publication of the International Association*
882 *of Sedimentologists*. Blackwell Publishing Ltd., pp. 167–193.
- 883 Berman, M., 1986. Testing for spatial association between a point process and another
884 stochastic process. *Applied Statistics* 35, 54–62.
- 885 Bernatchez, J. A., 2010. Taphonomic implications of orientation of plotted finds from
886 Pinnacle Point 13B (Mossel Bay, Western Cape Province, South Africa). *Journal of*
887 *Human Evolution* 59 (3–4), 274–288.
- 888 Bertran, P., Hetù, B., Texier, J.-P., Steijn, H. V., 1997. Fabric characteristics of subaerial
889 slope deposits. *Sedimentology* 44 (1), 1–16.
- 890 Bertran, P., Texier, J.-P., 1995. Fabric Analysis: Application to Paleolithic Sites. *Jour-*
891 *nal of Archaeological Science* 22 (4), 521–535.
- 892 Bevan, A., Crema, E., Li, X., Palmisano, A., 2013. Intensities, Interactions, and Un-
893 certainties: Some New Approaches to Archaeological Distributions. In: Bevan, A.,
894 Lake, M. (Eds.), *Computational Approaches to Archaeological Spaces*. Left Coast
895 Press, Walnut Creek, pp. 27–52.
- 896 Binford, L. R., 1981. Behavioral Archaeology and the "Pompeii Premise". *Journal of*
897 *Anthropological Research* 37 (3), 195–208.
- 898 Boschian, G., Saccà, D., 2010. Ambiguities in human and elephant interactions? Sto-
899 ries of bones, sand and water from Castel di Guido (Italy). *Quaternary International*
900 214 (1–2), 3–16.
- 901 Brantingham, P. J., Surovell, T. A., Waguespack, N. M., 2007. Modeling post-
902 depositional mixing of archaeological deposits. *Journal of Anthropological Archae-*
903 *ology* 26 (4), 517–540.
- 904 Carrer, F., 2015. Interpreting Intra-site Spatial Patterns in Seasonal Contexts: an Eth-
905 noarchaeological Case Study from the Western Alps. *Journal of Archaeological*
906 *Method and Theory*, 1–25.
- 907 Cobo-Sánchez, L., Aramendi, J., Domínguez-Rodrigo, M., 2014. Orientation patterns
908 of wildebeest bones on the lake Masek floodplain (Serengeti, Tanzania) and their
909 relevance to interpret anisotropy in the Olduvai lacustrine floodplain. *Quaternary*
910 *International* 322–323 (Supplement C), 277–284.
- 911 de la Torre, I., Benito-Calvo, A., 2013. Application of GIS methods to retrieve ori-
912 entation patterns from imagery; a case study from Beds I and II, Olduvai Gorge
913 (Tanzania). *Journal of Archaeological Science* 40 (5), 2446–2457.

- 914 Dibble, H. L., Chase, P. G., McPherron, S. P., Tuffreau, A., Oct. 1997. Testing the
915 reality of a "living floor" with archaeological data. *American Antiquity* 62 (4), 629–
916 651.
- 917 Diggle, P., 1985. A kernel method for smoothing point process data. *Applied Statistics*
918 (*Journal of the Royal Statistical Society, Series C*) 34, 138–147.
- 919 Domínguez-Rodrigo, M., Bunn, H., Mabulla, A., Baquedano, E., Uribelarrea, D.,
920 Pérez-González, A., Gidna, A., Yravedra, J., Diez-Martin, F., Egeland, C., Barba,
921 R., Arriaza, M., Organista, E., Ansón, M., 2014a. On meat eating and human evolution:
922 A taphonomic analysis of BK4b (Upper Bed II, Olduvai Gorge, Tanzania), and
923 its bearing on hominin megafaunal consumption. *Quaternary International* 322–323,
924 129–152.
- 925 Domínguez-Rodrigo, M., Bunn, H., Pickering, T., Mabulla, A., Musiba, C., Baque-
926 dano, E., Ashley, G., Diez-Martin, F., Santonja, M., Uribelarrea, D., Barba, R.,
927 Yravedra, J., Barboni, D., Arriaza, C., Gidna, A., 2012. Autochthony and orientation
928 patterns in Olduvai Bed I: a re-examination of the status of post-depositional biasing
929 of archaeological assemblages from FLK North (FLKN). *Journal of Archaeological
930 Science* 39 (7), 2116–2127.
- 931 Domínguez-Rodrigo, M., Cobo-Sánchez, L., Yravedra, J., Uribelarrea, D., Arriaza, C.,
932 Organista, E., Baquedano, E., 2017. Fluvial spatial taphonomy: a new method for the
933 study of post-depositional processes. *Archaeological and Anthropological Sciences*.
- 934 Domínguez-Rodrigo, M., Diez-Martín, F., Yravedra, J., Barba, R., Mabulla, A., Baque-
935 dano, E., Uribelarrea, D., Sánchez, P., Eren, M. I., 2014b. Study of the SHK Main
936 Site faunal assemblage, Olduvai Gorge, Tanzania: Implications for Bed II tapho-
937 nomy, paleoecology, and hominin utilization of megafauna. *Quaternary International*
938 322–323, 153–166.
- 939 Domínguez-Rodrigo, M., García-Pérez, A., 07 2013. Testing the Accuracy of Different
940 A-Axis Types for Measuring the Orientation of Bones in the Archaeological and
941 Paleontological Record. *PLoS ONE* 8 (7), e68955.
- 942 Domínguez-Rodrigo, M., Uribelarrea, D., Santonja, M., Bunn, H., García-Pérez, A.,
943 Pérez-González, A., Panera, J., Rubio-Jara, S., Mabulla, A., Baquedano, E., Yrave-
944 dra, J., Diez-Martín, F., 2014c. Autochthonous anisotropy of archaeological ma-
945 terials by the action of water: experimental and archaeological reassessment of the
946 orientation patterns at the Olduvai sites . *Journal of Archaeological Science* 41 (Sup-
947 plement C), 44–68.
- 948 Eberth, D. A., Rogers, R. R., Fiorillo, A. R., 2007. A practical approach to the study of
949 bonebeds. In: Rogers, R. R., Eberth, D. A., Fiorillo, A. R. (Eds.), *Bonebeds. Genesis,*
950 *Analysis, and Paleobiological Significance*. The University of Chicago Press, pp.
951 265–332.
- 952 Enloe, J. G., 2006. Geological processes and site structure: assessing integrity at a Late
953 Paleolithic open-air site in northern France. *Geoarchaeology* 21 (6), 523–540.

- 954 Eren, M. I., Durant, A., Neudorf, C., Haslam, M., Shipton, C., Bora, J., Korisettar,
955 R., Petraglia, M., 2010. Experimental examination of animal trampling effects on
956 artifact movement in dry and water saturated substrates: a test case from South India.
957 *Journal of Archaeological Science* 37 (12), 3010–3021.
- 958 Fernández-López, S. R., 1991. Taphonomic concepts for a theoretical biochronology.
959 *Revista Española de Paleontología* 6, 37–49.
- 960 Fiorillo, A. R., 1991. Taphonomy and depositional setting of Careless Creek Quarry
961 (Judith River Formation), Wheatland County, Montana, U.S.A. *Palaeogeography,*
962 *Palaeoclimatology, Palaeoecology* 81 (3), 281–311.
- 963 García-Moreno, A., Smith, G. M., Kindler, L., Pop, E., Roebroeks, W., Gaudzinski-
964 Windheuser, S., Klinkenberg, V., 2016. Evaluating the incidence of hydrological
965 processes during site formation through orientation analysis. A case study of the
966 middle Palaeolithic Lakeland site of Neumark-Nord 2 (Germany). *Journal of Ar-
967 chaeological Science: Reports* 6, 82–93.
- 968 Giusti, D., Arzarello, M., 2016. The need for a taphonomic perspective in spatial analy-
969 sis: Formation processes at the Early Pleistocene site of Pirro Nord (P13), Apricena,
970 Italy. *Journal of Archaeological Science: Reports* 8, 235–249.
- 971 Harvati, K., Panagopoulou, E., Tourloukis, V., Thompson, N., Karkanas, P., Athanas-
972 siou, A., Konidaris, G., Tsartsidou, G., Giusti, D., 2016. New Middle Pleistocene
973 elephant butchering site from Greece. In: Paleoanthropology Society Meeting. At-
974 lanta, Georgia, pp. A14–A15.
- 975 Hivernel, F., Hodder, I., 1984. Analysis of artifact distribution at Ngenym (Kenya):
976 depositional and postdepositional effects. In: Hietala, H., Larson, P. (Eds.), *Intrasite*
977 *Spatial Analysis in Archaeology*. Cambridge University Press, Ch. 7, pp. 97–115.
- 978 Hodder, I., Orton, C., 1976. *Spatial Analysis in Archaeology. New Studies in Archae-
979 ology*. Cambridge University Press, Cambridge.
- 980 Hovers, E., Ekshtain, R., Greenbaum, N., Malinsky-Buller, A., Nir, N., Yeshurun, R.,
981 2014. Islands in a stream? Reconstructing site formation processes in the late Middle
982 Paleolithic site of 'Ein Qashish, northern Israel. *Quaternary International* 331, 216–
983 233.
- 984 Isaac, G. L., 1967. Towards the interpretation of occupation debris: Some experiments
985 and observations. *Kroeber Anthropological Society Papers* 37 (37), 31–57.
- 986 Jammalamadaka, S., Sengupta, A., Sengupta, A., 2001. *Topics in Circular Statistics.*
987 Series on multivariate analysis. World Scientific.
- 988 Karkanas, P., Tourloukis, V., Thompson, N., Giusti, D., Panagopoulou, E., Harvati, K.,
989 this issue. Sedimentology and micromorphology of the Lower Palaeolithic lakeshore
990 site Marathousa 1, Megalopolis basin, Greece. *Quaternary International*.

- 991 Kluskens, S. L., 1990. Orientation and density analysis of stone artefacts at Combe-
992 Capelle Bas, Périgord, France. Master's thesis, University of Pennsylvania.
- 993 Konidaris, G., Athanassiou, A., Tourloukis, V., Thompson, N., Giusti, D.,
994 Panagopoulou, E., Harvati, K., this issue. The skeleton of a straight-tusked elephant
995 (*Palaeoloxodon antiquus*) and other large mammals from the Middle Pleistocene lo-
996 cality Marathousa 1 (Megalopolis Basin, Greece): preliminary results. Quaternary
997 International.
- 998 Krumbein, W. C., 1941. Measurement and geological significance of shape and round-
999 ness of sedimentary particles. Journal of Sedimentary Research 11 (2), 64–72.
- 1000 Lenoble, A., Bertran, P., 2004. Fabric of Palaeolithic levels: methods and implications
1001 for site formation processes. Journal of Archaeological Science 31 (4), 457–469.
- 1002 Lenoble, A., Bertran, P., Lacrampe, F., 2008. Solifluction-induced modifications
1003 of archaeological levels: simulation based on experimental data from a modern
1004 periglacial slope and application to French Palaeolithic sites. Journal of Archaeo-
1005 logical Science 35 (1), 99–110.
- 1006 Lindsay, J. F., 1968. The development of clast fabric in mudflows. Journal of Sedimen-
1007 tary Research 38 (4), 1242–1253.
- 1008 Macdonald, D. I. M., Jefferson, T. H., 1985. Orientation studies of waterlogged wood;
1009 a paleocurrent indicator? Journal of Sedimentary Research 55 (2), 235–239.
- 1010 Malinsky-Buller, A., Hovers, E., Marder, O., 2011. Making time: ‘Living floors’,
1011 ‘palimpsests’ and site formation processes – A perspective from the open-air Lower
1012 Paleolithic site of Revadim Quarry, Israel. Journal of Anthropological Archaeology
1013 30 (2), 89–101.
- 1014 Marwick, B., 2017. Computational reproducibility in archaeological research: Ba-
1015 sic principles and a case study of their implementation. Journal of Archaeological
1016 Method and Theory 24 (2), 424–450.
- 1017 Marwick, B., d'Alpoim Guedes, J., Barton, C. M., Bates, L. A., Baxter, M., Beavan,
1018 A., Bollwerk, E. A., Bocinsky, R. K., Brughams, T., Carter, A. K., Conrad, C.,
1019 Contreras, D. A., Costa, S., Crema, E. R., Daggett, A., Davies, B., Drake, B. L.,
1020 Dye, T. S., France, P., Fullager, R., Giusti, D., Graham, S., Harris, M. D., Hawks, J.,
1021 Heath, S., Huffer, D., Kansa, E. C., Kansa, S. W., Madsen, M. E., Melcher, J., Negre,
1022 J., Neiman, F. D., Opitz, R., Orton, D. C., Przystupa, P., Raviele, M., Riel-Salvatore,
1023 J., Riris, P., Romanowska, I., Smith, J., Strupler, N., Ullah, I. I., Vlack, H. G. V.,
1024 VanValkenberg, N., Watrall, E. C., Webster, C., Wells, J., Winters, J., Wren, C. D.,
1025 2017. Open science in archaeology. SAA Archaeological Record 17 (4), 8–14.
- 1026 McPherron, S. J., 2005. Artifact orientations and site formation processes from total
1027 station proveniences. Journal of Archaeological Science 32 (7), 1003–1014.
- 1028 McPherron, S. J., Dibble, H. L., Goldberg, P., 2005. Z. Geoarchaeology 20 (3), 243–
1029 262.

- 1030 Morton, A. G. T., 2004. Archaeological Site Formation: Understanding Lake Margin
1031 Contexts. Vol. 1211 of International Series. British Archaeological Reports, Oxford.
- 1032 Nickel, B., Riegel, W., Schonherr, T., Velitzelos, E., 1996. Environments of coal forma-
1033 tion in the Pleistocene lignite at Megalopolis, Peloponnesus (Greece) - reconstruc-
1034 tion from palynological and petrological investigations. N. Jb. Geol. Palaont. A. 200,
1035 201–220.
- 1036 Ohser, J., 1983. On estimators for the reduced second moment measure of point pro-
1037 cesses. Mathematische Operationsforschung und Statistik, series Statistics 14, 63–
1038 71.
- 1039 Organista, E., Domínguez-Rodrigo, M., Yravedra, J., Uribe Larrea, D., Arriaza, M. C.,
1040 Ortega, M. C., Mabulla, A., Gidna, A., Baquedano, E., 2017. Biotic and abiotic pro-
1041 cesses affecting the formation of BK Level 4c (Bed II, Olduvai Gorge) and their bear-
1042 ing on hominin behavior at the site. Palaeogeography, Palaeoclimatology, Palaeo-
1043 ecology (in press).
- 1044 Orton, C., 1982. Stochastic process and archaeological mechanism in spatial analysis.
1045 Journal of Archaeological Science 9 (1), 1–23.
- 1046 Panagopoulou, E., Tourloukis, V., Thompson, N., Athanassiou, A., Tsartsidou, G.,
1047 Konidaris, G., Giusti, D., Karkanas, P., Harvati, K., 2015. Marathousa 1: a new Mid-
1048 dle Pleistocene archaeological site from Greece. Antiquity Project Gallery 89 (343).
- 1049 Petraglia, M. D., Nash, D. T., 1987. The impact of fluvial processes on experimen-
1050 tal sites. In: Nash, D. T., Petraglia, M. D. (Eds.), Natural formation processes and
1051 the archaeological record. Vol. 352 of International Series. British Archaeological
1052 Reports, Oxford, pp. 108–130.
- 1053 Petraglia, M. D., Potts, R., 1994. Water Flow and the Formation of Early Pleistocene
1054 Artifact Sites in Olduvai Gorge, Tanzania . Journal of Anthropological Archaeology
1055 13 (3), 228–254.
- 1056 Pierson, T. C., 2005. Distinguishing between debris flows and floods from field evi-
1057 dence in small watersheds. USGS Numbered Series, U.S. Geological Survey.
- 1058 R Core Team, 2017. R: A Language and Environment for Statistical Computing. R
1059 Foundation for Statistical Computing, Vienna, Austria.
1060 URL <https://www.R-project.org/>
- 1061 Ripley, B., 1977. Modelling spatial patterns. Journal of the Royal Statistical Society,
1062 series B 39, 172–212.
- 1063 Ripley, B., 1988. Statistical inference for spatial processes. Cambridge University
1064 Press.
- 1065 Ripley, B. D., 1976. The second-order analysis of stationary point processes. Journal
1066 of Applied Probability 13 (2), 255–266.

- 1067 Ripley, B. D., 1981. *Spatial Statistics*. John Wiley and Sons, New York.
- 1068 Schick, K. D., 1984. Processes of paleolithic site formation: an experimental study.
1069 Ph.D. thesis, University of California, Berkeley.
- 1070 Schick, K. D., 1986. Stone Age sites in the making: experiments in the formation
1071 and transformation of archaeological occurrences. Vol. 319 of International Series.
1072 British Archaeological Reports, Oxford.
- 1073 Schick, K. D., 1987. Modeling the formation of Early Stone Age artifact concentra-
1074 tions. *Journal of Human Evolution* 16, 789–807.
- 1075 Schiffer, M. B., 1972. Archaeological Context and Systemic Context. *American Antiquity*
1076 37 (2), 156–165.
- 1077 Schiffer, M. B., 1983. Toward the identification of formation processes. *American Antiquity*
1078 48 (4), 675–706.
- 1079 Schiffer, M. B., 1987. Formation processes of the archaeological record. University of
1080 New Mexico Press, Albuquerque.
- 1081 Shackley, M. L., 1978. The behaviour of artefacts as sedimentary particles in a fluvial environment. *Archaeometry* 20 (1), 55–61.
- 1082 Sánchez-Romero, L., Benito-Calvo, A., Pérez-González, A., Santonja, M., 12 2016.
1083 Assessment of Accumulation Processes at the Middle Pleistocene Site of Ambrona
1084 (Soria, Spain). Density and Orientation Patterns in Spatial Datasets Derived from
1085 Excavations Conducted from the 1960s to the Present. *PLOS ONE* 11 (12), 1–27.
- 1086 Texier, J.-P., 2000. A propos des processus de formation des sites préhistoriques / About
1087 prehistoric site formation processes. *Paléo* 12 (1), 379–386.
- 1088 Toots, H., 1965. Orientation and distribution of fossils as environmental indicators. In:
1089 Nineteenth Field Conference of the Wyoming Geological Association. pp. 219–292.
- 1090 Tourloukis, V., Thompson, N., Panagopoulou, E., Giusti, D., Konidaris, G., Karkanas,
1091 P., Harvati, K., this issue. Lithic and osseous artifacts from the Lower Palaeolithic
1092 site of Marathousa 1, Megalopolis, Greece: preliminary results. *Quaternary Interna-*
1093 *tional*.
- 1094 van Vugt, N., de Bruijn, H., van Kolfschoten, M., Langereis, C. G., 2000. Magneto-
1095 and cyclostratigraphy and mammal-fauna's of the Pleistocene lacustrine Megalopo-
1096 lis Basin, Peloponnesos, Greece. *Geologica Ultrajectina* 189, 69–92.
- 1097 Vaquero, M., Chacón, M. G., García-Antón, M. D., de Soler, B. G., Martínez, K.,
1098 Cuartero, F., 2012. Time and space in the formation of lithic assemblages: The
1099 example of Abric Romaní Level J. *Quaternary International* 247 (0), 162–181.
- 1100 Villa, P., 2004. Taphonomy and stratigraphy in european prehistory. *Before Farming*
1101 2004 (1), 1–20.

- 1103 Voorhies, M., 1969. Taphonomy and population dynamics of an early Pliocene ver-
1104 tebrate fauna, Knox County, Nebraska. Contributions to Geology, University of
1105 Wyoming Special Paper 1, 1–69.
- 1106 Walter, M. J., Trauth, M. H., 2013. A MATLAB based orientation analysis of
1107 Acheulean handaxe accumulations in Olorgesailie and Kariandusi, Kenya Rift. Jour-
1108 nal of Human Evolution 64 (6), 569–581.
- 1109 Wood, R. W., Johnson, D. L., 1978. A survey of disturbance processes in archaeologi-
1110 cal site formation. In: Schiffer, M. B. (Ed.), Advances in archaeological method and
1111 theory. Vol. 1. Academic Press, Ch. 9, pp. 315–381.
- 1112 Woodcock, N., Naylor, M., 1983. Randomness testing in three-dimensional orientation
1113 data. Journal of Structural Geology 5 (5), 539–548.